blood

2011 118: 3039-3050
doi:10.1182/blood-2011-04-349746 originally published online July 26, 2011

Homeostatic cytokines orchestrate the segregation of CD4 and CD8 memory T-cell reservoirs in mice

Lili Yang, Yang Yu, Manorama Kalwani, Tai-Wei Joy Tseng and David Baltimore

Blood (print ISSN 0006-4971, online ISSN 1528-0020), is published weekly by the American Society of Hematology, 2021 L St, NW, Suite 900, Washington DC 20036.

Homeostatic cytokines orchestrate the segregation of CD4 and CD8 memory T-cell reservoirs in mice

Lili Yang,[1] Yang Yu,[1] Manorama Kalwani,[1] Tai-Wei Joy Tseng,[1] and David Baltimore[1]

[1]Division of Biology, California Institute of Technology, Pasadena, CA

Memory T cells (T_Ms) have been detected in many tissues but their quantitative distribution remains largely undefined. We show that in mice there is a remarkably biased accumulation of long-term CD4 T_Ms into mucosal sites (mainly gut, especially Peyer patches), and CD8 T_Ms into lymph nodes and spleen (in particular, peripheral lymph nodes [PLNs]). This distinction correlates with their differentiated expression of PLN- and gut-homing markers. CD8 and CD4 T_Ms selectively require the expression of PLN-homing marker CCR7 or gut-homing marker α4β7 for maintenance. PLNs and gut supply CD8 and CD4 T_Ms with their individually favored homeostatic cytokine, IL-15, or IL-7. Cytokine stimulation in turn regulates the different gut-homing marker expression on CD4 and CD8 T_Ms. IL-15 plays a major role in vivo regulating CD8 T_Ms homing to PLNs. Thus, the reservoir segregation of CD4 and CD8 T_Ms meets their individual needs for homeostatic cytokines and is under feedback control of cytokine stimulation. (*Blood*. 2011; 118(11):3039-3050)

Introduction

A prominent feature of T-cell immunity is the formation of memory T cells (T_Ms) after exposure to infectious agents, leading to more effective immune protection on re-encountering the same stimulus.[1] CD4 and CD8 T cells carry out distinct immunologic functions: while CD8 T cells are specialized for cytotoxicity,[2] CD4 T cells play a more comprehensive role through helping CD8 T cells and B cells to respond and generate memory,[3,4] and through constituting specialized compartments like T_H17 cells and T regulatory cells.[5,6] CD4 and CD8 T cells show considerable differences in their memory generation and maintenance.[7-10] For example, CD8 T_M differentiation appears to be efficient and follows a linear differentiation pathway, whereas CD4 T_M differentiation is more complex and requires a prolonged period of stimulation.[8] In the absence of antigen, T_Ms are maintained mainly through interactions with homeostatic cytokines, with CD8 T_Ms particularly depending on IL-15 while CD4 T_Ms primarily depend on IL-7.[10]

Homeostatic cytokines are mainly produced by nonhematopoietic tissue cells and considered to be supplied largely in a tissue-restricted manner in limited amount.[11,12] T_Ms need to home to special "niches" to efficiently access and compete for these survival factors.[13,14] The search for such "niches" and the associated reservoir distribution for T_Ms has been severely hampered by the technical difficulty of systemically tracking and quantifying T_Ms.[9,11] Recently, bone marrow (BM) has been proposed as an important reservoir for both CD8 and CD4 T_Ms, which is considered to contain niches defined by IL-7–expressing stromal cells.[15-17] However, the systemic distribution of T_M reservoirs, especially the direct comparison between CD4 and CD8 T_M reservoirs, remains largely unexamined.

In the past decade, the increasing application of molecular imaging techniques for studying the immune system has yielded valuable insights into the dynamics of the immune cells.[18-20] Among them, BLI is especially suitable for studying T-cell trafficking in small animal models, because of its capacity for noninvasive measurement of T-cell dynamics in vivo, its excellent signal-to-noise ratios, and its user-friendly and relatively inexpensive instrumentation.[20]

Aided by the BLI technique, we have systemically analyzed and compared the reservoir distribution of long-term CD4 and CD8 T_Ms in mice. We find that although both T_Ms are found in multiple tissues, their preferences for individual tissues are quite different: CD8 T_Ms accumulate mainly in lymph nodes and spleen, particularly PLNs whereas CD4 T_Ms accumulate preferentially in mucosal sites, mainly gut and especially Peyer patches (PPs). This polarized accumulation correlates with their differing expression of PLN- and gut-homing markers. Deficiency of a gut-homing marker α4β7 or a PLN-homing marker CCR7 selectively impairs the formation and maintenance of CD4 or CD8 T_Ms. PLNs produce high level of IL-15, making them particularly fit as a home for CD8 T_Ms while gut expresses IL-7, making it appropriate for CD4 T_Ms. In addition, IL-7 and IL-15 stimulation sustains the differentiated expression of homing markers on the CD4 and CD8 T_Ms, providing an apparent feedback control to stabilize their reservoir segregation.

Methods

Mice and materials, antibodies and flow cytometry, tissue lymphocytes isolation, DC-directed lentivirus infection, CD4 effector T cells (T_Es) differentiation in vitro, CD4 memory T cells (T_Ms) functional analysis, and IL-7 and IL-15 mRNA tissue expression are provided in supplemental Methods (available on the *Blood* Web site; see the Supplemental Materials link at the top of the online article). All mouse experiments were approved by the California Institute of Technology Institutional Animal Care and Use Committee.

Submitted April 18, 2011; accepted July 7, 2011. Prepublished online as *Blood* First Edition paper, July 26, 2011; DOI 10.1182/blood-2011-04-349746.

The online version of this article contains a data supplement.

The publication costs of this article were defrayed in part by page charge payment. Therefore, and solely to indicate this fact, this article is hereby marked "advertisement" in accordance with 18 USC section 1734.

MFG retrovirus

The MFG construct was generated by inserting into the MSCV retroviral vector[21] the Fluc and EGFP genes linked by a P2A sequence.[22] Retroviruses were made using HEK293.T cells as previously described.[21]

Effector T cell (T_E) culture, transduction, MACS sorting and adoptive transfer

To generate polyclonal T_Es, SP, and LN cells harvested from B6 female mice were cultured in T-cell culture media containing 0.5 μg/mL anti–mouse CD3 and 0.5 μg/mL anti–mouse CD28 (Biolegend) for 3 days. To generate antigen-specific T_Es, SP, and LN cells harvested from OT1 or OT2 Tg mice were cultured in T-cell culture medium containing either 0.1 μg/mL $OVAp_{257-269}$ or 1 μg/mL $OVAp_{323-339}$ for 3 days. To generate MFG-labeled T_Es, on day 1 and day 2 of the culture, T cells were spin-infected with retroviral supernatant supplemented with 10 μg/mL polybrene for 90 minutes at 770*g* at 30°C. CD4 and CD8 T_Es were purified using MACS sorting through positive-selection (Miltenyi Biotec). For adoptive transfer, purified CD4 or/and CD8 T_Es ($2\text{-}20 \times 10^6$/recipient), supplemented with freshly isolated BM cells ($5\text{-}10 \times 10^6$/recipient), were injected intravenously into recipient mice that had received 1000 rads of total body irradiation. Postadoptive transfer, the recipient mice were maintained on the mixed antibiotic sulfmethoxazole and trimethoprim oral suspension (Hi-Tech Pharmacal) for 4 weeks.

Bioluminescence imaging

Bioluminescence imaging (BLI) was performed using an IVIS200 imaging system (Xenogen/Caliper LifeSciences). Live animal imaging was acquired 5 minutes after intraperitoneal injection of D-Luciferin (1 mg/mouse, Xenogen/Caliper Lifesciences). To image tissues, mice that received intraperitoneal injection of D-Luciferin (3 mg/mouse) were dissected 5 minutes after injection; the individual tissues were imaged within the following 15 minutes. Imaging results were analyzed using a Living Imaging 2.50 software.

In vitro and in vivo cytokine stimulation for T_Ms

For in vitro stimulation, CD4 or CD8 T_Ms were cultured in T-cell culture media supplemented with 100 ng/mL of either IL-7 or IL-15 for 3 days. For in vivo stimulation, each mouse received a single intraperitoneal injection of 10 μg of either IL-7 or IL-15 once daily for 5 sequential days.

Statistical analyses

Student *t* test was used for paired comparisons. Data are presented as mean ± SEM, unless otherwise indicated.

Results

Visualizing the segregation of CD4 and CD8 T_M reservoirs in mice

To track T_Ms in mice, we constructed a dual-reporter retroviral vector, MFG, coexpressing firefly luciferase (FLuc) and enhanced green fluorescence protein (EGFP; Figure 1A). OVA-specific CD4 (OT2) and CD8 (OT1) effector T cells (T_Es) were generated in vitro, transduced with MFG, separately transferred into albino B6 recipient mice and tracked in vivo using BLI (supplemental Figure 1A). This approach allowed us to visualize the formation of T_Ms in an antigen-free host developing from a relatively homogeneous and synchronized population of T_Es.[21,23-24] Estimation of the pool size of the transferred cells by measuring the total body luminescence (TBL) of a recipient mouse divided T_M formation into 3 phases: expansion (weeks 1-3), contraction (week 4) and stabilization (> 1 month; Figure 1B,C), which closely resembles the T_M formation kinetics during an acute infection.[25] FACS analysis confirmed that both OT2 and OT1 T cells at the stabilization phase have acquired the typical T_M phenotype: $CD25^-CD69^-CD62L^{hi/lo}CD44^{hi}$ (supplemental Figure 1B).

In the early expansion phase (weeks 1 and 2), OT2 and OT1 T cells exhibited similar disseminated distribution patterns: they were initially detected in the lung (as early as 14 hours after transfer), probably because lung is the first organ they enter on exiting the heart (Figure 1B and supplemental Figure 2A), followed by movement to many other lymphoid and nonlymphoid tissues, including lymph nodes (LNs), spleen (SP), bone marrow (BM), liver, pancreas (Pan), thymus (Thy), genital tract (GT) and gut (supplemental Figure 2B). Differences in distribution patterns appeared in the later expansion phase (week 3), became evident during the contraction phase (week 4), and were maintained throughout the stabilization phase (> 1 month), for as long as the T_Ms were detectable (up to 1 year in our experiments; Figure 1B-D). Comparison of individual tissues for OT2 and OT1 T_M accumulation showed that they could be classified into 4 groups (Figure 1D): (1) OT1 T_M-favored reservoirs, which included peripheral LNs (PLNs), mesenteric LNs (MLNs) and SP, showing ~ 3-5 fold higher total luminescence (TL) for OT1 T_Ms than OT2 T_Ms; (2) common reservoirs, which included BM, lung, and liver, showing similar TL levels; (3) OT2 T_M-favored reservoirs, which included mucosal sites like gut and genital tract, showing ~ 5- to 10-fold higher TL signals for OT2 T_Ms than OT1 T_Ms; and (4) un-favored reservoirs, which included all other tissues.

Overall, the OT1 T_Ms preferentially accumulated in LNs and SP, particularly PLNs; whereas OT2 T_Ms preferred to accumulate in mucosal sites including genital tract and gut, with gut containing the most OT2 T_Ms because of its large size. Imaging of the isolated gut showed that OT2 T_Ms distributed through the entire gut tract from stomach to colon, with PPs identified as "hot spots" containing highly concentrated OT2 T_Ms (Figure 1E). Quantification of the TL in gut sub-regions showed that the small intestine, appendix/cecum, stomach and colon contained ~ 80%, 10%, 5%, and 5% of the gut OT2 T_Ms, respectively (Figure 1E).

Because OT2 and OT1 T cells were specific for a model Ag, OVA, we asked whether this distinct T_M homing pattern was general or unique to this Ag. When MFG-labeled polyclonal CD4 and CD8 T_Es were transferred into albino B6 recipients (supplemental Figures 1C-D), the resulting CD4 and CD8 T_Ms showed a similar segregated accumulation (Figure 1F), suggesting that it was a general feature of long-term T_Ms independent of their Ag specificity. FACS analysis also confirmed that in the stabilization phase, both the MFG-labeled polyclonal CD4 and CD8 T cells displayed typical T_M phenotype $CD25^-CD69^-CD44^{hi}CD62L^{hi/lo}$ (supplemental Figure 1D).

Various types of CD4 and CD8 T_Ms show a similar polarized tissue distribution

Because BLI is only a semi-quantitative method, we further analyzed the tissue distribution of polyclonal CD4 and CD8 T_Ms generated through adoptive transfer of effector T cells using flow cytometry. When equal numbers of B6 CD4 and CD8 T_Es were cotransferred into Thy1.1 congenic recipient mice, the resulting CD4 and CD8 T_Ms generated in the recipients exhibited different $CD4T_M/CD8T_M$ ratios in individual tissues. In agreement with the BLI study, scoring individual tissues by calculating the $\log_2$ of their $CD4T_M/CD8T_M$ ratios classified them into "CD8 T_M-favored reservoirs" that had negative scores (including PLN, peripheral blood, MLN and SP), "common reservoirs" that had scores close to zero (including BM and lung), and "CD4 T_M-favored reservoirs"

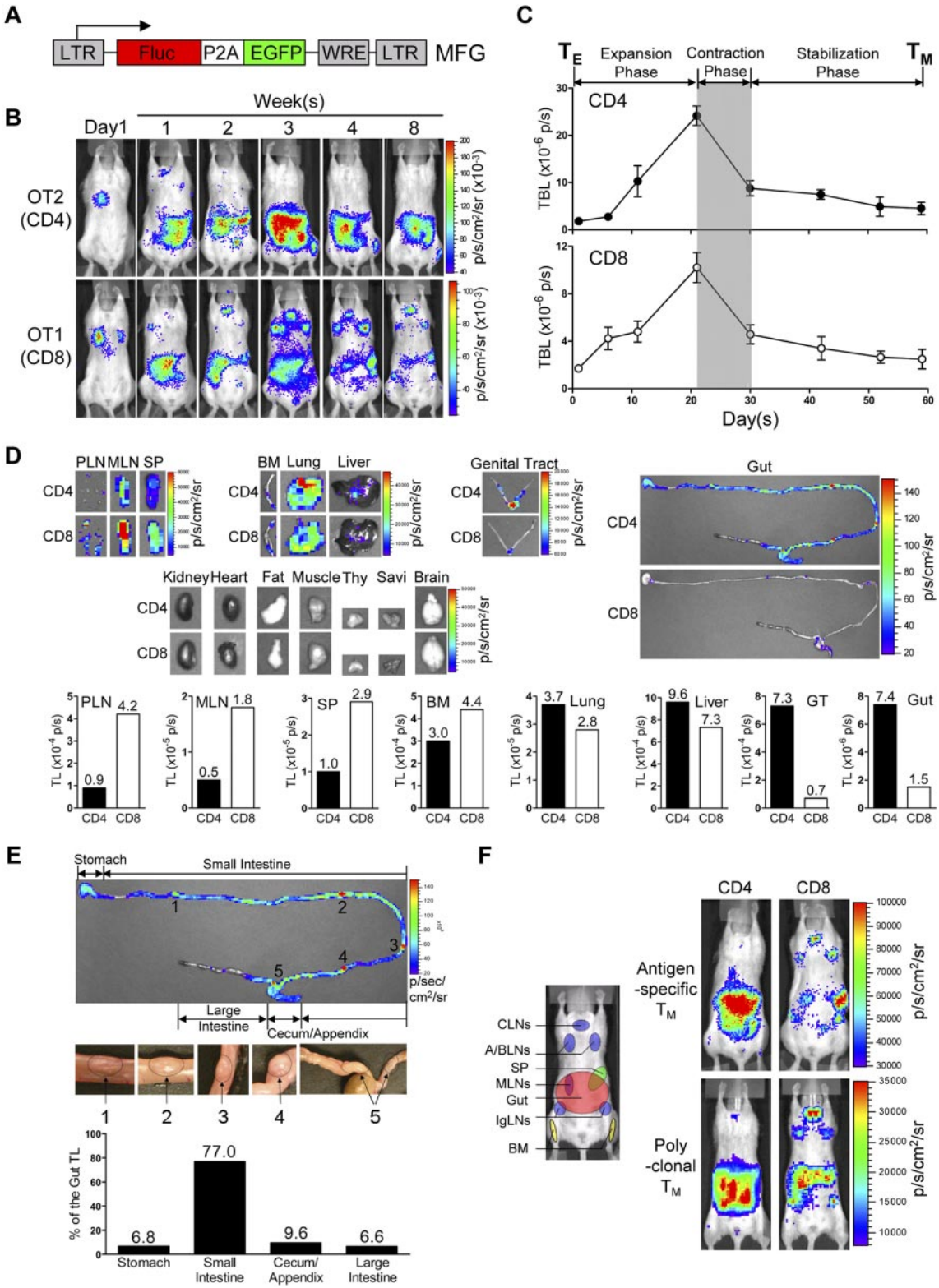

Figure 1. Visualizing the segregation of CD4 and CD8 T_M reservoirs in mice. (A) Schematic representation of dual-reporter retrovector MFG. LTR indicates long-term repeats; Fluc, firefly luciferase; P2A, porcine teschovirus 2A sequence; EGFP, enhanced green fluorescence protein; and WRE, woodchuck responsive element. (B,C) Visualization of the CD4 and CD8 T_M formation in albino B6 mice postadoptive transfer of 1×10^6 MFG-labeled OT2 (CD4) or OT1 (CD8) effector T cells (T_Es) using BLI. Representative BLI images (B) and the measurements of total body luminescence (TBL, mean ± SEM; C) are shown (n = 4). Shaded area marks contraction phase (C). (D,E) Visualization of the CD4 and CD8 T_Ms in individual tissues using excised tissue BLI. (D) Tissues were collected from albino B6 recipient mice 2 months after transfer of 10×10^6 MFG-labeled OT2 (CD4) or OT1 (CD8) T_Es. PLN indicates peripheral lymph node; MLN, mesenteric LN; SP, spleen; BM, bone marrow; Thy, thymus; GT, genital tract; and Savi, salivary gland. (E) Detailed analysis of CD4 T_M homing to gut. BLI images of the gut tract (top, the "hot spots" are numbered), identification of the "hot spots" as Peyer patches (PPs; middle), and the measurements of luminescence in gut sub-regions (bottom) are shown. Data are representative of 3 independent experiments. (F) Visualization of the antigen-specific or polyclonal CD4 and CD8 T_Ms formed in albino B6 recipient mice each receiving 1×10^6 either MFG-labeled OT2 or OT1 T_Es, or MFG-labeled B6 CD4 or CD8 T_Es using BLI. Representative BLI images collected 1 month after transfer are shown (n = 4). Schematic showing the individual tissue localization in mice is provided for reference. CLNs indicate cervical LNs; A/BLNs, axillary/brachial LNs; and IgLN, inguinal LNs. PLNs refer to the combination of CLNs, A/BLNs, and IgLNs.

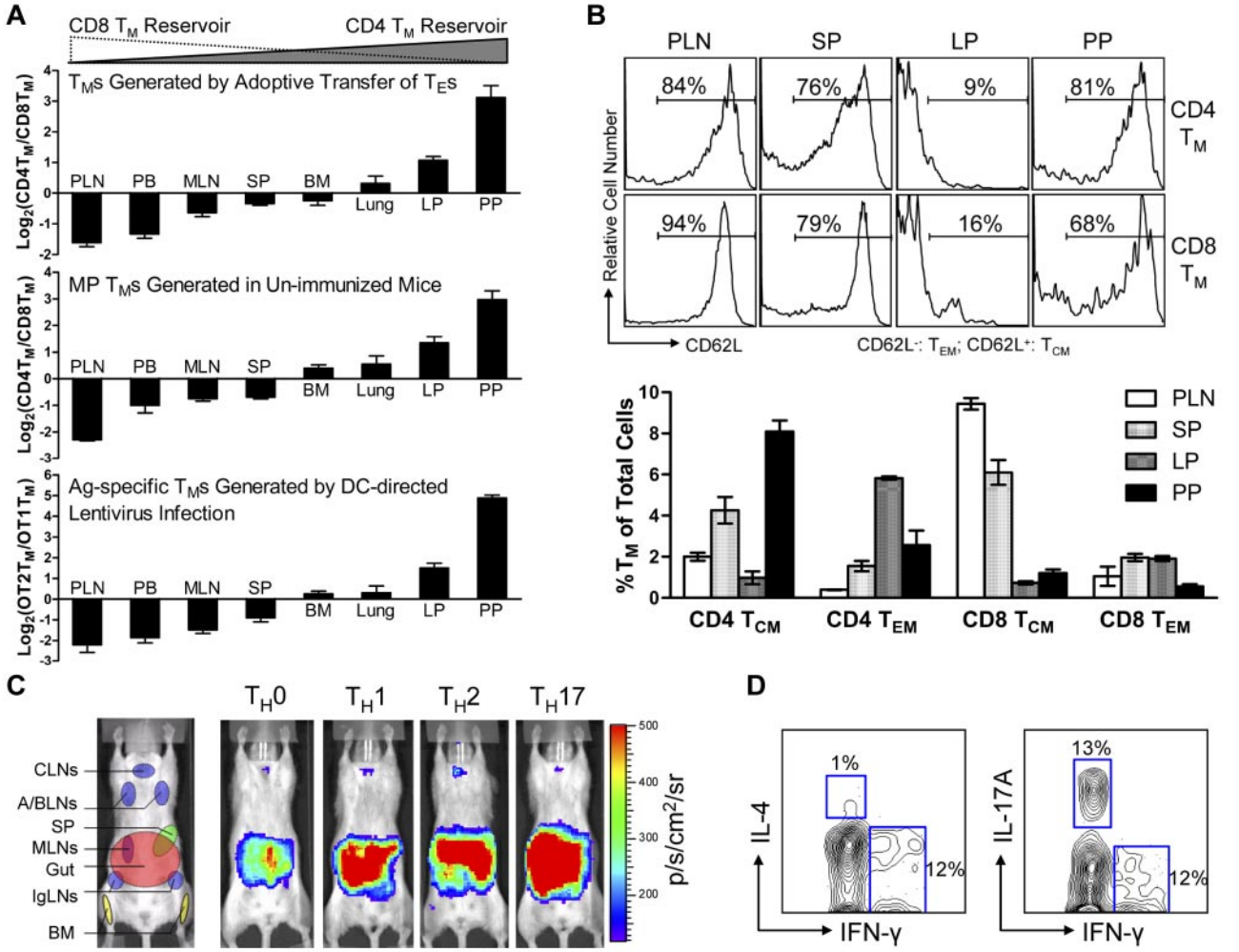

Figure 2. Various types of CD4 and CD8 T_Ms show a similar polarized tissue distribution. (A) Tissue distribution of CD4 and CD8 T_Ms of various originalities. Top: CD4 and CD8 T_Ms (gated as Thy1.2$^+$CD4$^+$ and Thy1.2$^+$CD8$^+$, respectively) generated in the Thy1.1 congenic mice 2 months after transfer of a mix of equal number (10×10^6) of B6 CD4 and CD8 T_Es; middle: memory-phenotype (MP) CD4 T_Ms (gated as CD4$^+$CD25$^-$CD44^{hi}, CD25 staining was included to gate off Tregs) and CD8 T_Ms (gated as CD8$^+$TCRβ$^+$CD44^{hi}, TCRβ staining was included to gate off the CD8$^+$ nonαβ T cells present in some tissues) spontaneously generated in 1-year-old B6 mice (similar results were observed for B6 mice aged from 3 months to 1 year); and bottom: OVA antigen-specific OT2 T_Ms (gated as CD4$^+$CD25$^-$TCRVβ5$^+$CD44^{hi}, CD25 staining was included to gate off Tregs) and OT1 T_Ms (gated as CD8$^+$TCRVβ5$^+$CD44^{hi}) generated in OT2 or OT1 transgenic mice 2 months after infection with 1×10^8 TU DC-directed lentivirus expressing OVA antigen. Data are presented as mean ± SEM (n = 4). (B) Tissue distribution of CD4 and CD8 T_{CM}s and T_{EM}s. Various tissues were harvested from 1-year-old B6 mice and analyzed for the presence of MP CD4 and CD8 T_{CM}s and T_{EM}s (gated as CD4$^+$CD25$^-$CD44^{hi}CD62L$^+$, CD4$^+$CD25$^-$CD44^{hi}CD62L$^-$, CD8$^+$TCRβ$^+$CD44^{hi}CD62L$^+$, or CD8$^+$ TCRβ$^+$CD44^{hi}CD62L$^-$, respectively) using flow cytometry. Histogram plots (top) and quantification of T_Ms (bottom) are shown. Data are presented as mean ± SEM (n = 4). T_{CM}s indicates central memory T cells; and T_{EM}s, effector memory T cells. (C) Visualization of the CD4 T_Ms formed in the abino B6 mice each receiving 1×10^6 MFG-labeled CD4 T_Es that had been differentiated in vitro into T_H0, T_H1, T_H2, or T_H17 cells using BLI. Representative BLI images collected 2 months after adoptive transfer are shown (n = 4). Schematic showing the individual tissue localization in mice is provided for reference. (D) Functional analysis of MP CD4 T_Ms residing in PPs of 1-year-old B6 mice. PP cells (pool of 4 mice) were stimulated with PMA + Ionomycin in vitro for 6 hours and analyzed for the cytokine production of CD4 T_Ms (gated as CD4$^+$CD44$^+$) using flow cytometry. Contour plots representative of 3 independent experiments are shown.

that had positive scores (including the lamina propria [LP] and PP in gut; Figure 2A top and supplemental Figure 3A). In particular, PLN and PP had the lowest (~ −1.8) and highest (~ 3) scores, confirming that they were the most polarized reservoirs for CD8 and CD4 T_Ms, respectively. Interestingly, a low score (−1.5) for peripheral blood was obtained, showing more CD8 T_Ms in circulation.

We further used this scoring method to study the tissue distribution of the CD4 and CD8 T_Ms developed endogenously in unperturbed mice using flow cytometry. Both memory-phenotype (MP) T_Ms spontaneously generated in aged mice[10] (Figure 2A middle and supplemental Figure 3B) and the antigen-specific T_Ms induced in vivo through infecting OT1 and OT2 transgenic mice with a DC-directed lentivirus that expresses OVA antigen[26] (Figure 2A bottom and supplemental Figure 3C) showed a similarly polarized tissue distribution of CD4 and CD8 T_Ms. Importantly, this distinct reservoir distribution is unique for memory CD4 and CD8 T cells, because a similar analysis of naive CD4 and CD8 T cells (T_Ns) revealed a much different distribution pattern (supplemental Figure 3E), suggesting that a unique homing propensity is acquired during memory formation.

Because T_Ms are heterogeneous in regard to their phenotype and functionality,[7,9,27] we also studied the tissue distribution of T_M subtypes. Based on their expression of CD62L and CCR7, both CD4 and CD8 T_Ms can be divided into T_{CM}s and T_{EM}s.[28,29] Despite the classic definition that T_{CM}s home to LNs while T_{EM}s home to peripheral tissues, analysis of MP CD4 and CD8 T_{EM}s (CD62L$^-$) and T_{CM}s (CD62L$^+$) in aged mice revealed the presence of both T_{EM}s and T_{CM}s in all the tissues that we studied, although at various ratios (Figure 2B and supplemental Figure 3F). Of note, in addition to the overall gut-tropic accumulation for CD4 T_Ms and LN/SP-tropic accumulation of CD8 T_Ms, there are slightly differed tissue

preferences for individual subsets: PPs for CD4 T_{CM}s, LP for CD4 T_{EM}s, PLNs for CD8 T_{CM}s, and SP for CD8 T_{EM}s. CD4 T_Ms can also be divided into various subtypes based on their differentiated functions.[9] Differentiating CD4 T_Es in vitro into T_H0, T_H1, T_H2, and T_H17 cells followed by adoptively transferring them into recipients resulted in CD4 T_Ms that all predominantly accumulated in gut (Figure 2C), implying that gut might be the common dominant reservoir for CD4 T_Ms of various functions.[24] This notion is further supported by the observation that in aged mice, the MP CD4 T_Ms harvested from PPs contained subsets that exhibited cytokine production profiles featured for T_H1 (IFN-γ^+IL-4^-), T_H2 (IFN-γ^-IL-4^+), and T_H17 (IFN-γ^-IL-$17A^+$; Figure 2D).

CD4 and CD8 T_Ms differ on their expression of PLN- and gut-homing markers

The observation of the extremely polarized gut-tropic versus PLN-tropic accumulation of CD4 and CD8 T_Ms raised 2 interesting questions: how do the T_Ms achieve this distinct distribution and what might be the rationale for them to accumulate in these 2 separate tissues? To address the first question, we examined the expression of several tissue-specific homing markers on CD4 and CD8 T_Ms, which have been well documented to control T_M traffic to specific tissues.[7,30-32] We were particularly interested in the best characterized PLN-homing markers CCR7 and CD62L,[33,34] and the gut-homing markers CCR9 and $\alpha4\beta7$.[35,36] Examination of the MP T_Ms in the spleen of aged mice revealed that both T_Ms expressed similar levels of CCR7 and CD62L, but CD4 T_Ms expressed much more homogenous and higher levels of CCR9 and $\alpha4\beta7$ than CD8 T_Ms (Figure 3A). The major difference of $\alpha4\beta7$ expression stems from the expression of $\beta7$ (Figure 3A), its more "gut-specific" component.[36] This PLN- and gut-homing marker expression correlates with their gut-tropic and PLN-tropic accumulation, and was unique for CD4 and CD8 T_Ms, because it was not observed for T_Ns and T_Es (Figure 3A). Further studies of antigen-specific or polyclonal T_Ms generated through adoptive transfer of in vitro differentiated T_Es or Ag-specific T_Ms generated through DC-directed lentivirus infection all confirmed a PLN- and gut-homing marker expression pattern similar to MP T_Ms (supplemental Figure 4A).

In addition, we also analyzed the MP T_Ms for their expression of other homing markers that have been indicated to play a role in T_M trafficking, including CCR4, CCR5, CCR6, CCR10, CXCR3, and CXCR4.[30] Different expressions of several markers were observed, indicating their possible roles in regulating the T_M reservoir distribution as well (supplemental Figure 4B).

We then tracked the homing marker expression on CD4 and CD8 T cells during their transition from T_Es to T_Ms in recipient mice postadoptive transfer. Both CD4 and CD8 T cells initially expressed all the LN-homing and gut-homing markers in the expansion phase (weeks 1-3; Figure 3C), correlating well with their similar and ubiquitous presence in various tissues at this stage (Figure 3B and supplemental Figure 4C). During the contraction phase (week 4), the critical "turning point" for memory formation, the CD4 T cells continued up-regulating their expression of both LN and gut-homing markers while the CD8 T cells started down-regulating their gut-homing markers (Figure 3C). This change correlated with a sharp increase of CD8 T cells in PLN, in concert with the continuous accumulation of CD4 T cells in the gut, eventually leading to the highly polarized tissue distribution of CD4 and CD8 T cells as they finished the transition into T_Ms and entered the stabilization phase (Figure 3B and supplemental Figure 4C). Therefore, despite their similar expression of PLN-homing markers, the biased tissue accumulation of CD4 and CD8 T_Ms seems to correlate with their differentiated expression of gut homing markers, which is gradually acquired as they transit from effector to memory T cells.

CD4 and CD8 T_Ms selectively require the expression of gut- or PLN-homing marker for their formation and maintenance

We then sought to determine whether the expression of appropriate gut- or PLN-homing markers is required for the formation and maintenance of CD4 and CD8 T_Ms. Analysis of mice genetically ablated for a major PLN-homing marker CCR7[33] revealed that compared with the age-matched wild-type (WT) mice, they had a markedly reduced MP CD8 T_M population (especially in the PLNs), but a relatively normal CD4 T_M population, shown in both the $CD4T_M/CD8T_M$ ratio plot (Figure 4A) and the absolute T_M counts (Figure 4B). On the contrary, mice deficient for a major gut-homing marker $\beta7$ (which results in a deficiency of $\alpha4\beta7$)[37] had the opposite phenotype of reduced CD4 but relatively normal CD8 T_Ms (Figure 4A-B). Because both CCR7KO and $\beta7$KO mice have other deficiencies in the immune system that may affect their generation of MP T_Ms in vivo,[33,37] we extracted T cells from these mice, generated MFG-labeled CD4 and CD8 T_Es in vitro, and then adoptively transferred them into WT recipients. This experimental design allowed us to confine the CCR7 or $\beta7$ deficiency to the differentiated T_Es. Quantification of the T_Ms formed in the recipient mice confirmed the previous findings: CCR7 or $\beta7$ deficiency selectively impaired the formation of CD8 or CD4 T_Ms, respectively, but had little effect on the other (Figure 4C). Notably, the surviving CCR7KO CD8 T_Ms mainly resided in gut but not PLNs, indicating an indispensable role of CCR7 for mediating PLN-tropic accumulation of CD8 T_Ms. In contrast, the surviving $\beta7$KO CD4 T_Ms still mostly remained in gut, suggesting that gut-tropic accumulation of CD4 T_Ms was not solely dependent on $\alpha4\beta7$ (Figure 4C). Thus, our data imply that CD4 and CD8 T_Ms selectively require the expression of gut- or PLN-homing markers, in particular $\alpha4\beta7$ and CCR7, for their formation and maintenance.

CD4 and CD8 T_Ms accumulate in tissues that supply them with their favored homeostatic cytokines

Next, we examined the physiologic relevance of the separate CD4 and CD8 T_Ms accumulation in gut and PLNs. Considering the notable difference between CD4 and CD8 T_Ms of their dependence on the homeostatic cytokines IL-7 and IL-15,[10] we hypothesized that the distinct tissue distribution of CD4 and CD8 T_Ms might meet their individual needs. CD4 and CD8 T_Ms expressed similar level of IL-7 receptor (composed of γc and IL-7Rα chains), while CD8 T_Ms expressed much higher and more homogenous level of IL-15 receptor (evident by a modestly higher level of IL-15Rα and a significantly higher level of IL-2/15Rβ [CD122]; Figure 5A). This distinction was T_M-specific because the differences between CD4 and CD8 T_Ns and T_Es were much smaller (supplemental Figure 5A). Tracking IL-2/15Rβ expression on CD4 and CD8 T cells during their effector to memory transition showed CD8 T cells maintaining a constant high expression of IL-2/15Rβ while CD4 T cells gradually down-regulated its expression (supplemental Figure 5B). Stimulating the purified T_Ms in vitro with either IL-7 or IL-15 showed that CD8 T_Ms generally had a proliferation advantage over CD4 T_Ms, especially when IL-15 was present (Figure 5B). When IL-7 or IL-15 was injected into mice harboring MFG-labeled CD4 or CD8 T_Ms, we found that IL-7 induced a $\sim$ 2.7-fold expansion of CD8 T_Ms and a $\sim$ 2-fold expansion of CD4 T_Ms, whereas IL-15 induced a striking $\sim$ 20-fold expansion of

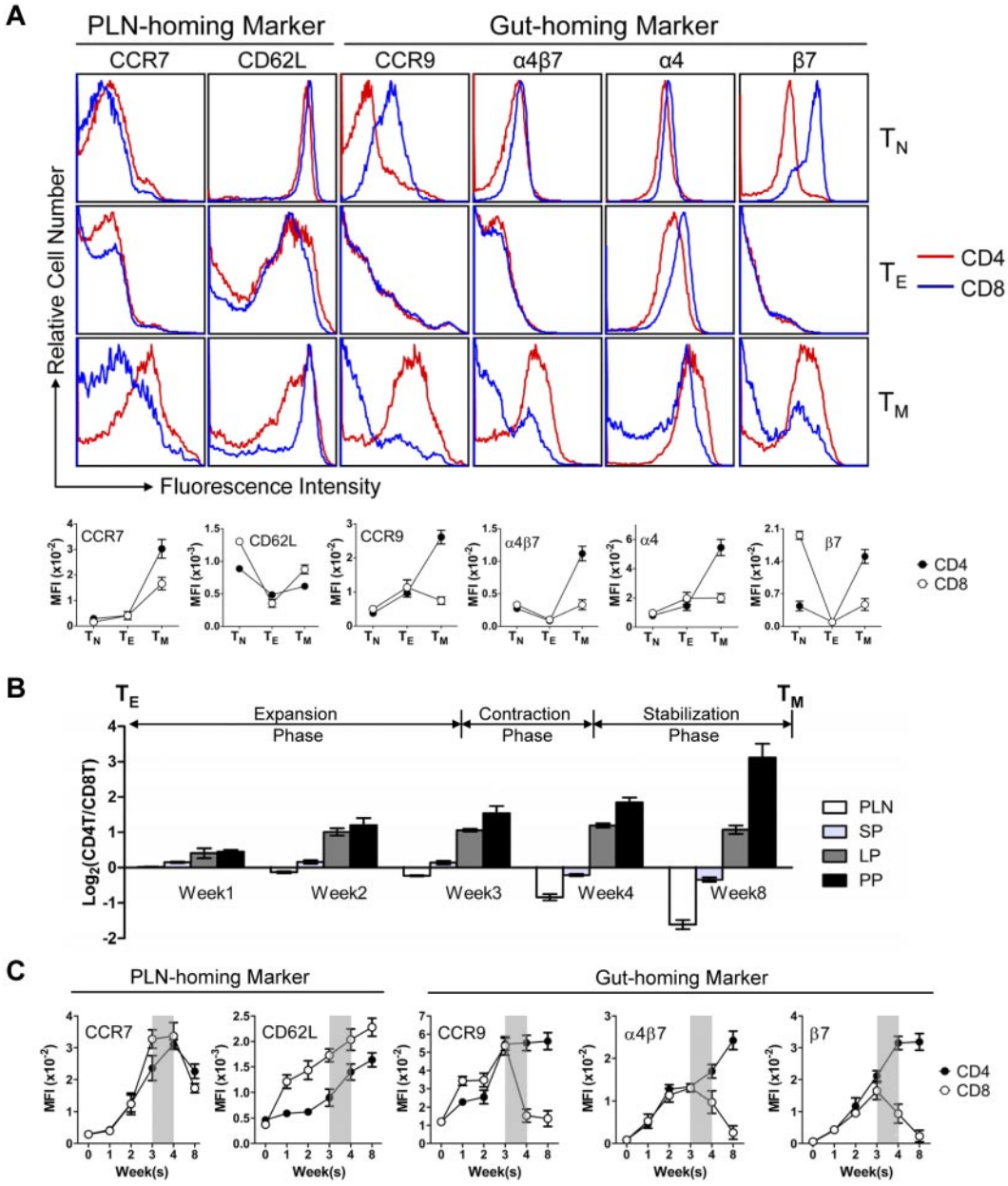

Figure 3. CD4 and CD8 T_Ms differ on their expression of gut-homing markers. (A) Homing marker expression on naive (T_N), effector (T_E), and memory (T_M) CD4 and CD8 T cells analyzed by flow cytometry. CD4 and CD8 T_Ns (gated as $CD4^+CD25^-CD44^{lo}$ and $CD8^+$ $CD44^{lo}$, respectively) and T_Ms (gated as $CD4^+CD25^-CD44^{hi}$ and $CD8^+CD44^{hi}$, respectively) were naive or memory T cells detected in the spleen of 1-year-old B6 mice. T_Es were generated by stimulating B6 spleen T cells in vitro with anti-CD3 and anti-CD28 for 3 days. Representative histogram plots (top) and measurements of mean fluorescence intensity (MFI; mean ± SEM; bottom) are shown (n = 8). (B,C) Time-course tracking of CD4 and CD8 T cells (gated as $Thy1.2^+CD4^+$ and $Thy1.2^+CD8^+$, respectively) for their tissue homing preference (B) and homing marker expression (C) during their transition from T_Es to T_Ms in Thy1.1 congenic mice receiving adoptive transfer of a mix of equal number (10×10^6) of B6 CD4 and CD8 T_Es. (B) Data are presented as mean ± SEM. (C) Representative homing marker expression on spleen T cells detected by flow cytometry, shown as mean fluorescence intensity (MFI; mean ± SEM). N = 4. Shaded area marks contraction phase.

CD8 T_Ms and only a ~2-fold expansion of CD4 T_Ms (Figure 5C-D). Examination of the tissue-specific expression of IL-7 and IL-15 revealed a relatively homogenous expression of IL-7 in various tissues with some preference for gut, while IL-15 was expressed at notably higher level in PLN (Figure 5E). This distribution makes PLN a particularly attractive reservoir site for the IL-15–dependent CD8 T_Ms. Therefore, our results supported a "homing to fitness" hypothesis: IL-15–dependent CD8 T_Ms tend to accumulate in PLNs, the site particularly rich in IL-15 whereas the IL-7–dependent CD4 T_Ms tend to accumulate in the gut where they are provided with IL-7 and do not need to compete with CD8 T_Ms for cytokines.

Homeostatic cytokines regulate the differentiated expression of gut-homing markers on CD4 and CD8 T_Ms in vitro

In addition to their role in maintaining T_M homeostasis, we were interested to explore whether homeostatic cytokines might also regulate T_M homing molecule expression. To this end, we purified the MP CD4 and CD8 T_Ms from B6 mice and cultured them in vitro in the presence or absence of IL-7 or IL-15. Without cytokines in the culture, the difference in gut-homing marker expression was almost extinguished (Figure 6A), implying that the differentiation was not fixed for T_Ms but was rather actively acquired through their constant interaction with external signals, such as homeostatic

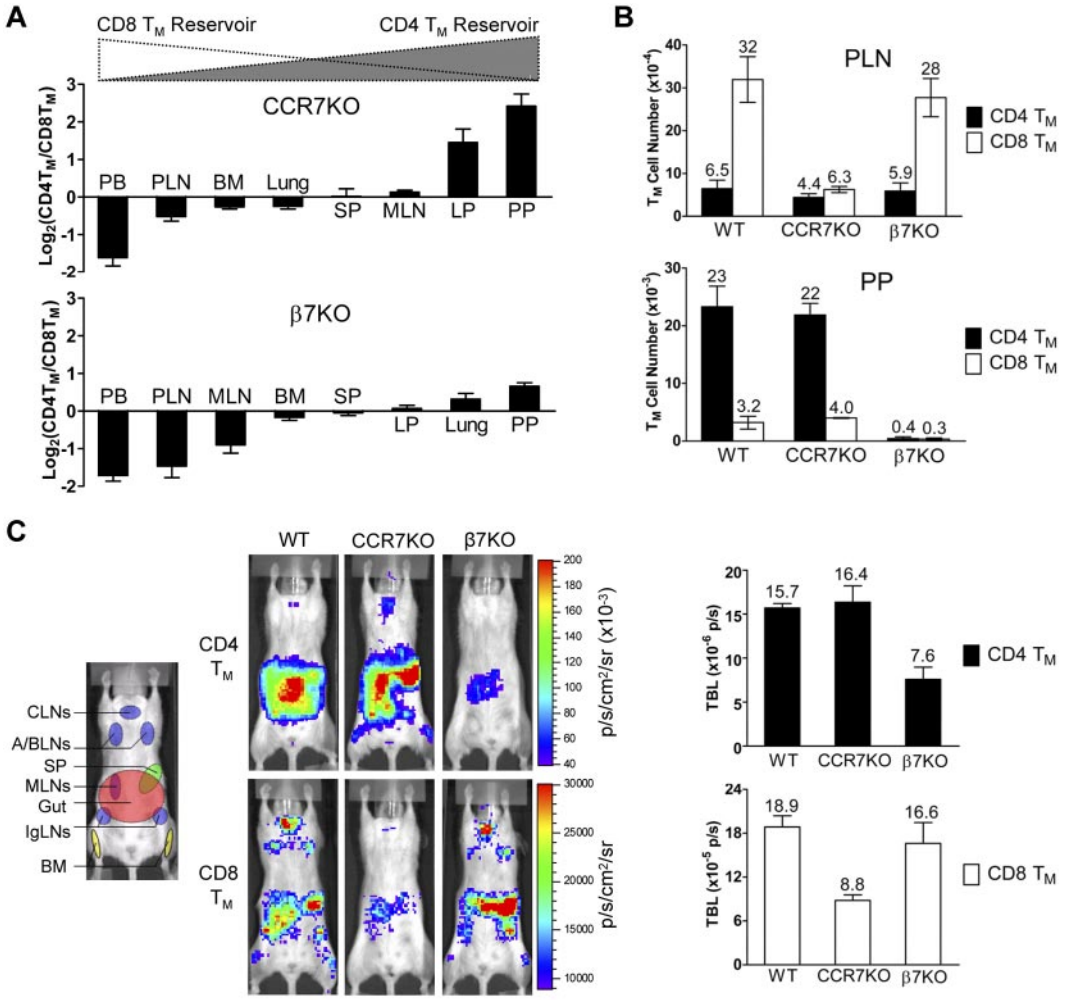

Figure 4. CD4 and CD8 T_Ms selectively require the expression of α4β7 or CCR7 for their formation and maintenance. (A) Tissue accumulation of MP CD4 and CD8 T_Ms (gated as $CD4^+CD25^-CD44^{hi}$ and $CD8^+$ $TCR\beta^+CD44^{hi}$, respectively) in 10-month-old CCR7KO or β7KO mice. Data are presented as mean ± SEM (n = 4). (B) Comparison of CD4 and CD8 T_M number in PLN and PP of 10-month-old wild-type (WT), CCR7KO and β7KO mice. Data are presented as mean ± SEM (n = 4). (C) Study of the influence of CCR7 or β7 deficiency on CD4 and CD8 T_M formation using BLI. Either MFG-labeled CD4 T_Es (5×10^6) or CD8 T_Es (1×10^6) of the indicated genotype were adoptively transferred into albino B6 recipient mice. Representative BLI images and total body luminescence (TBL) measurements of the indicated recipients (mean ± SEM, n = 4) 1 month after transfer are shown.

cytokines. Indeed, their differential marker expression was partly restored when IL-7 was added to the culture medium and, more strikingly, was almost restored to the in vivo level when IL-15 was added (Figure 6A). This regaining of the differentiation worked through reversely up-regulating or down-regulating gut homing markers on CD4 and CD8 T_Ms (including both CCR9 and α4β7), similarly to what was observed during the T_E to T_M transition (Figure 3C). This regulation was specific for gut homing markers because the PLN-homing marker CD62L was up-regulated on both CD4 and CD8 T_Ms in response to either IL-7 or IL-15 stimulation (Figure 6A). Notably, we observed that both IL-7 and IL-15 stimulation specifically promoted the CD8 T_Ms, but not CD4 T_Ms, to significantly up-regulate IL-2/15Rβ, thereby providing a positive-feedback control to maintain the different responsiveness to IL-15 between CD4 and CD8 T_Ms (Figure 6A). Thus, our results indicate that in addition to their capacity to maintain T_M survival and proliferation, the homeostatic cytokines, especially IL-15, appears to also regulate the distinct homing of CD4 and CD8 T_Ms by maintaining their differential expression of gut-homing markers. This regulation seems to stem from an intrinsic difference between CD4 and CD8 T_Ms as to their response to homeostatic cytokine stimulation.

IL-15 plays a major role in regulating CD8 T_Ms homing to PLNs in vivo

In light of the in vitro study, we further asked whether homeostatic cytokines, in particular IL-15, might regulate T_M homing in vivo. First we studied the T_M distribution in the IL-15KO mice. Consistent with a previous report,[38] we found that compared with WT mice, IL-15KO mice have a much reduced number of MP CD8 T_Ms, but their CD4 T_Ms were relatively unaffected. Although there was a general reduction of CD8 T_Ms in all the tissues that we analyzed, the most significant reduction occurred in the CD8 T_M-favored reservoirs, especially in PLNs, resulting in a much less dramatically polarized distribution of the CD4 and CD8 T_Ms. Supplementing the IL-15KO mice with IL-15 greatly expanded their CD8 T_Ms. In addition, there was a corrected preference for CD8 T_M to accumulate in PLNs, shown as a more significant increase of CD8 T_Ms in PLNs compared with their increases in the other tissues, which partially restored the polarized tissue distribution of CD4 and CD8 T_Ms (Figures 6B-C and supplemental Figure 6B). These finding correlated with the observation that in IL-15KO mice, the CD8 T_Ms expressed high levels of gut-homing markers CCR9 and α4β7 similar to CD4 T_Ms (supplemental Figure 6A).

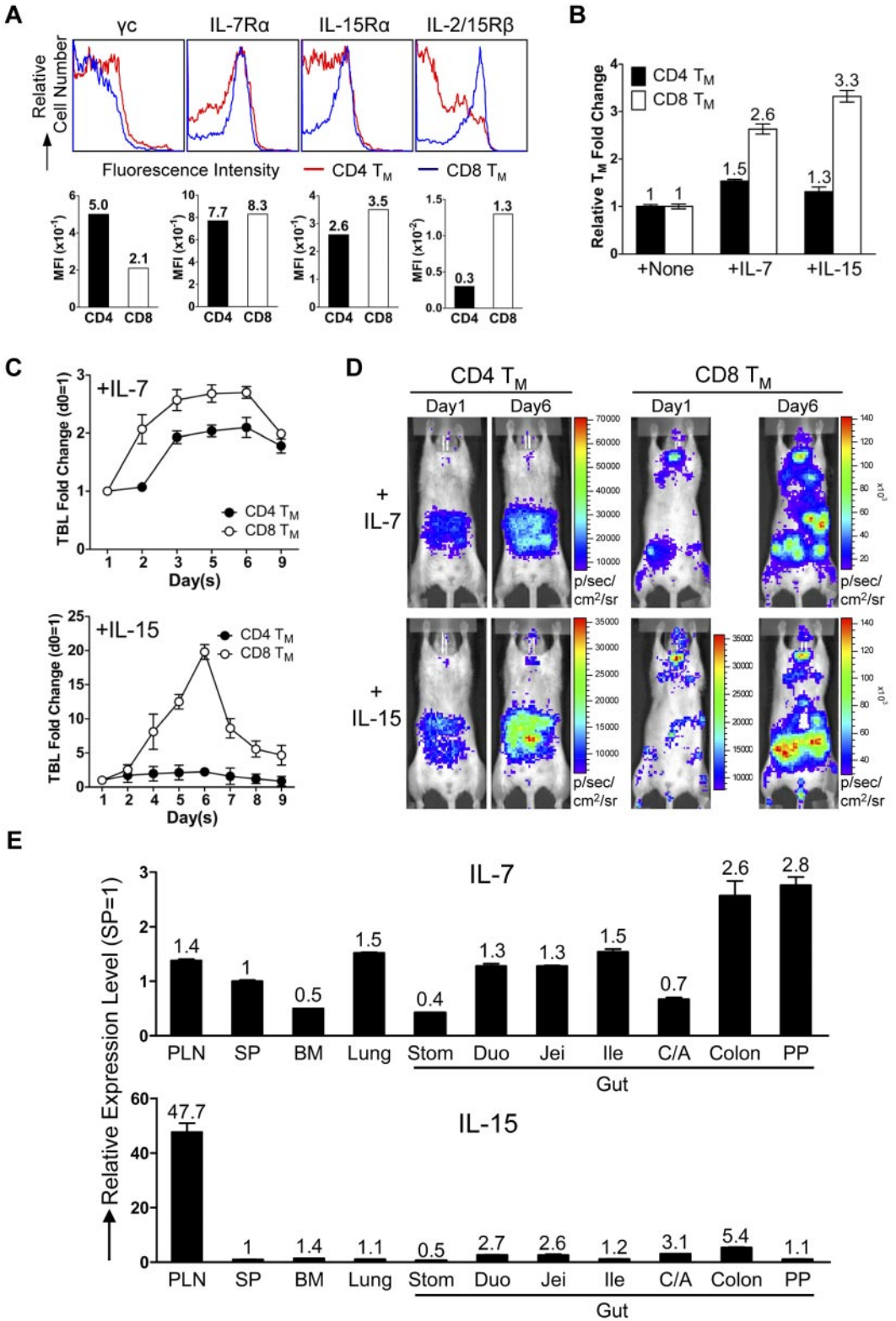

Figure 5. CD4 and CD8 T_Ms home to tissues that supply them with their favored homeostatic cytokines. (A) Cytokine receptor expression on the MP CD4 and CD8 T_Ms (gated as $CD4^+CD25^-CD44^{hi}$ and $CD8^+CD44^{hi}$, respectively) in the spleen of 1-year-old B6 mice measured by flow cytometry. Representative histogram plots and mean fluorescence intensity (MFI) measurements are shown ($n > 4$). (B) Proliferation of CD4 and CD8 T_Ms in response to cytokine stimulation (100 ng/mL) for 3 days in vitro measured by cell counts. T_Ms were purified from 1-year-old B6 mice. Representative data are presented as mean of triplicates ± SEM ($n = 4$). (C,D) Proliferation of CD4 and CD8 T_Ms in response to cytokine stimulation in vivo measured by BLI. MFG-labeled OT2 (CD4) or OT1 (CD8) T_Es (1×10^6) were adoptively transferred into each albino B6 recipient mouse. Six months later, the recipients harboring the OT2 or OT1 T_Ms received administration (IP) of either IL-7 or IL-15 daily (10 μg) for 5 sequential days. (C) Time-course tracking of the TBL change of the indicated recipient mice receiving either IL-7 or IL-15. Data are presented as mean ± SEM. (D) Representative BLI images of the indicated mice right before the 1st cytokine administration (day 1) and 1 day after the last cytokine administration (day 6; $n = 3$-4). (E) Tissue expression of IL-7 and IL-15 in 1-year-old B6 mice measured by Taqman Q-PCR. Representative data are presented as mean of triplicates ± SEM ($n = 4$).

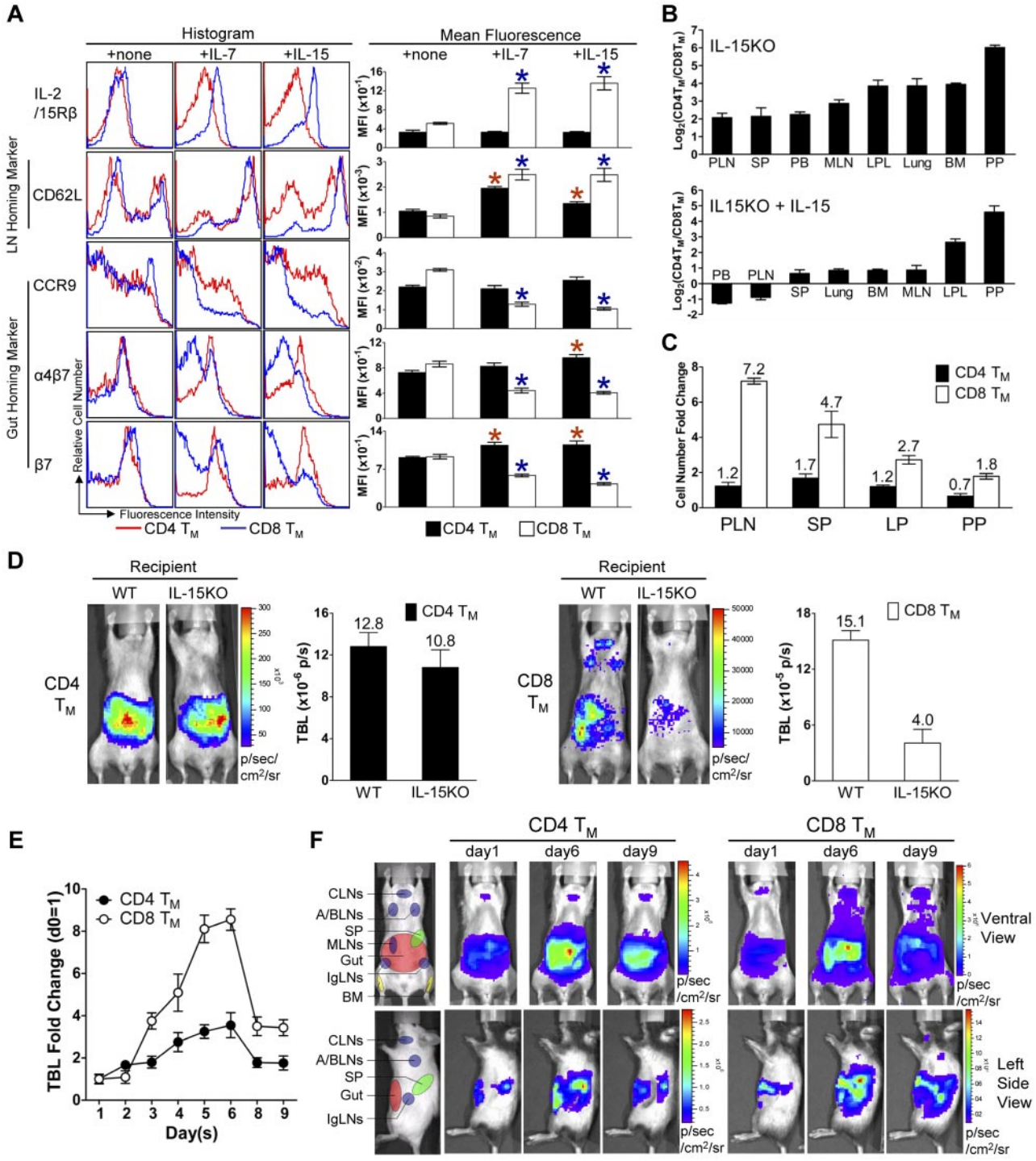

Figure 6. Homeostatic cytokines regulate the differentiated expression of gut-homing markers on CD4 and CD8 T_Ms in vitro and in vivo. (A) IL-7 and IL-15 regulation of homing marker expression on MP CD4 and CD8 T_Ms in vitro. MP CD4 and CD8 T_Ms (gated as $CD4^+CD25^-CD44^{hi}$ or $CD8^+CD44^{hi}$, respectively) purified from the spleen of 1-year-old B6 mice (pool of 8 mice) were cultured in triplicates in vitro for 3 days in the presence or absence of 100 ng/mL of IL-7 or IL-15. Their expression of homing markers, as well as IL-2/15Rβ (CD122), was measured by flow cytometry. Data are shown as histogram plots and measurements of mean fluorescence intensity (MFI, presented as mean of triplicates ± SEM), and are representative of at least 3 independent experiments. Red or blue $^*P < .05$ (CD4 or CD8 T_Ms cultured with cytokine compared with CD4 or CD8 T_Ms cultured without cytokine). (B-C) Quantification of MP CD4 and CD8 T_Ms (gated as $CD4^+CD25^-CD44^{hi}$ and $CD8^+TCR\beta^+CD44^{hi}$, respectively) in 9-month-old IL-15KO mice with or without supplementation of IL-15 (IP 10μg daily for 5 sequential days). (B) Tissue distribution of CD4 and CD8 T_Ms. (C) The fold changes of CD4 and CD8 T_M numbers in response to IL-15 treatment in indicated tissues. Data are shown as mean ± SEM (n = 3). (D) Comparison of CD4 and CD8 T_M formation in WT or IL-15KO mice using BLI. MFG-labeled B6 CD4 or CD8 T_Es (1×10^6) were adoptively transferred into either WT (B6) or IL-15KO recipient mice. Representative BLI images and the measurements of TBL (shown as mean ± SEM) of the indicated recipients collected 1 month after transfer are shown (n = 3). (E,F) The impact of IL-15 supplement on the homeostasis and homing of CD4 and CD8 T_Ms studied using BLI. MFG-labeled WT (B6) CD4 or CD8 T_Es (5×10^6) were transferred into IL-15KO recipient mice. One month later, the recipients were supplemented with IL-15 (IP 10μg daily for 5 sequential days). (E) Time-course tracking of the fold change of TBL of the indicated recipients. Data are presented as mean ± SEM. (F) Representative BLI images of the indicated recipients on day 1 (right before the 1st IL-15 administration), day 6, and day 9. N = 4. Schematics showing the individual tissue localization in mice (ventral view and left side view) are provided for reference.

When IL-15 was supplemented, the difference in gut-homing marker expression was largely restored between CD4 and CD8 T_Ms, mainly through down-regulating these markers on CD8 T_Ms (supplemental Figure 6A). Meanwhile, the PLN-homing marker CD62L was up-regulated on CD8 T_Ms, indicating that the down-regulation was specific for gut-homing markers (supplemental Figure 6A). Moreover, the difference of IL-2/15Rβ expression on CD4 and CD8 T_Ms was greatly reduced in IL-15KO mice, and was significantly restored on IL-15 supplementation, suggesting that IL-15 might provide a major positive feedback control in vivo to differentiate CD4 and CD8 T_Ms in their responsiveness to IL-15 (supplemental Figure 6A).

To further study the role of IL-15 as a tissue-restricted factor to regulate CD8 T_M homing to PLN, we adoptively transferred MFG-labeled WT CD4 and CD8 T_Es into either WT or IL-15KO recipients, and then follow their T_M formation in vivo. The results corroborated the previous findings that mice lacking IL-15 did not effectively support CD8 T_M formation, especially their homing to PLNs, whereas the maintenance and homing of CD4 T_Ms was mostly unaffected (Figure 6D). Supplementation with IL-15 induced a significant expansion of CD8 T_Ms and promoted their homing to the PLNs, while limited expansion was seen for the CD4 T_Ms (Figure 6E-F). Taken together, our results indicate that IL-15 supplied by the tissues plays a major role in the regulation of CD8 T_M homing to PLNs in vivo. This conclusion is further supported by the finding that in WT mice, the MP CD4 and CD8 T_Ms harvested from PLNs where IL-15 expression is most abundant showed a more dramatic distinction of gut homing marker expression compared with those T_Ms harvested from SP (supplemental Figure 6C).

Discussion

Despite the detection of CD4 and CD8 T_Ms in many tissues,[1,32,39] a dynamic and systemic study of the localization of CD4 and CD8 T_Ms has been lacking, probably because of the difficulty of quantifying T_Ms, in particular CD4 T_Ms, in tissues outside the dedicated lymphoid organs. Taking advantage of BLI for its capacity to visualize the T_Ms in a live animal and in its excised organs, and combining it with direct measurements, we have attempted to provide a global picture of CD4 and CD8 T_M localization. We find a remarkably segregated tissue distribution of long-term CD4 and CD8 T_Ms in mice. Therefore in addition to their differences in functionality, anatomic localization is another important distinction between these 2 classes of T_Ms.

The accumulation of CD8 T_Ms mainly in the classic lymphoid organs (LNs and SP) was to be expected because they have long been recovered from these sites but the extremely specific accumulation of CD4 T_Ms in mucosal sites, particularly gut, and their relative paucity in LNs and SP was striking. The finding of gut as a major site for CD4 T_M homing is consistent with a previous study using whole body immunohistology to study CD4 T_M distribution in mice post protein antigen immunization.[39] However, despite the documentation of CD4 T_Ms being abundant in mucosal sites in mice, nonhuman primates and humans,[31,40] it has not been so evident that these sites represent specialized dominant reservoirs for CD4 T_Ms. What might be the physiologic rationale for the immune system to place these 2 types of T_Ms in almost complementary positions? Considering the different functions that CD4 and CD8 T_Ms serve,[8,9] it is conceivable that this distribution pattern allows them to together cover the major portals for sensing pathogens that enter the body, potentially providing effective immuno-surveillance. In fact, this distribution may facilitate their specific functional activities: localization of CD8 T_Ms in draining LNs and SP allows them to react quickly to dendritic cells that sample the invading pathogens in tissues or in the circulation and differentiate into effector cytotoxic T cells (CTLs) that can cleanse infected tissues; localization of CD4 T_Ms to mucosal sites would allow them to most efficiently respond to pathogens in these sites by both defending against them directly and helping the local B cells to produce antibodies protecting the mucosal surface. It should be noted that certain pathogens take advantage of this T_M distribution to aid their infection process. One example is SIV/HIV that primarily targets the CCR5-positive CD4 T_Ms and uses mucosal sites as its main entry route.[40] Massive infection and depletion of CD4 T_Ms in gut precedes the infection of other tissues, and is the most profound T-cell population abnormality in AIDS.[41-43] That gut is the predominant reservoir for CD4 T_Ms helps to explain the HIV/SIV tissue tropism, emphasizing the importance of providing mucosal protection in the design of therapeutic or vaccination strategies against HIV.

What is the physiologic significance for CD4 and CD8 T_Ms to separately accumulate in gut or PLNs? T_Ms depend on homeostatic cytokines for long-term survival, with CD8 T_Ms heavily reliant on IL-15 while CD4 T_Ms mainly respond to IL-7.[10] Our study of tissue production of these cytokines revealed a relatively homogenous expression of IL-7 among the tissues (albeit slightly higher in gut) but a much higher expression of IL-15 in PLNs. Therefore, it seems that CD8 T_Ms do benefit from accumulating in PLNs for easy access to IL-15. Meanwhile, the CD4 T_Ms in gut have access to IL-7 and avoid a direct competition with CD8 T_Ms for cytokines. Interestingly, commensal microflora have recently been shown to promote intestinal epithelia cells to produce IL-7,[44] implying that these microbes may play a role in the maintenance of CD4 T_Ms and their accumulation at mucosal sites. This notion is supported by our observation that in germ-free mice, in contrast to a relative constant level of memory-phenotype CD8 T_Ms, there is a significant reduction of CD4 T_Ms, especially in the gut (supplemental Figure 7). Importantly, we found that homeostatic cytokine stimulation of CD4 and CD8 T_Ms actively regulates their expression of homing markers, providing a potent feedback control for stabilizing their distinct homing pattern. In particular, IL-15 appears to play the dominant role by greatly down-regulating the expression of gut-homing markers on CD8 T_Ms. Indeed, depriving or supplementing IL-15 in vivo regulates the capacity of CD8 T_Ms to home to PLNs. Notably, the expression of IL-15 receptor, particularly its β subunit (IL-2/15Rβ or CD122), is quite different between CD4 and CD8 T_Ms and is also subjected to cytokine feedback control, strengthening their differentiated needs for IL-15.

In Figure 7, we bring together all of our observations into a "Memory Compartmentalization Model." Key to the model is that the memory development process programs CD4 and CD8 T_Ms into different regulatory pathways so that they respond differently to the hematopoietic cytokines. In the absence of cytokine stimulation, there is little difference between CD4 and CD8 T_Ms for their homing marker expression ($CD62L^{lo}CCR9^{hi}\alpha4\beta7^{hi}$). The cytokines up-regulate the PLN-homing marker CD62L on both T_Ms, but greatly down-regulate the gut-homing markers CCR9 and α4β7 on CD8 T_Ms ($CD62L^{hi}CCR9^{lo}\alpha4\beta7^{lo}$) while further up-regulate these markers on CD4 T_Ms ($CD62L^{hi}CCR9^{hi}\alpha4\beta7^{hi}$). This distinction of gut-homing marker expression leaves CD8 T_Ms to accumulate in

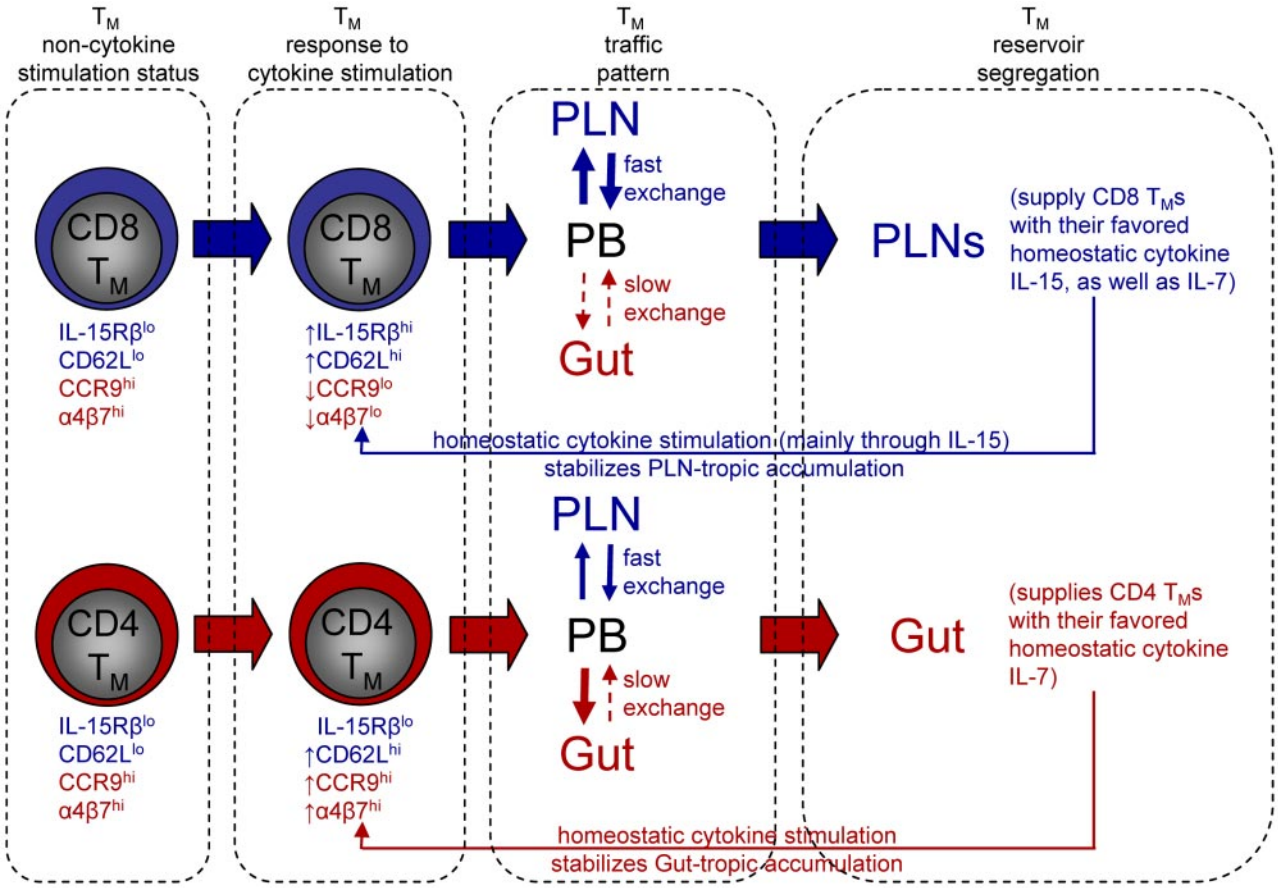

Figure 7. Memory compartmentalization model. This schematic model illustrates the segregation of CD4 and CD8 T_M reservoirs in mice, and the possible molecular controls and physiologic relevance of this phenomenon (for details, see main text).

PLNs by default. We postulate that CD4 T_Ms accumulate in gut because of their relative free exchange between PLNs and circulation but a more restricted exchange back to circulation once they enter the gut, as suggested by previous report.[45] It is relevant to point out that expression of certain tissue homing marker on T_Ms allow them to access the corresponding tissue and stay in that tissue for certain time, but by no means making them the permanent residents of that tissue. Instead, all T_Ms retain their capacity to survey the body through blood and lymphoid circulation. In the PLNs, CD8 T_Ms find a high level of their favored cytokine IL-15, while in the gut, CD4 T_Ms find an environment rich in their favored cytokine IL-7 which they can access without competing with CD8 T_Ms. The cytokine stimulation in turn stabilizes the PLN-tropic and gut-tropic accumulation of CD8 and CD4 T_Ms through down-regulating or up-regulating their gut-homing markers, respectively. In addition, the cytokine stimulation also maintains the different expression of IL-2/15Rβ on CD4 and CD8 T_Ms, strengthening their different reliance on IL-15. We should point out that this model mainly addresses T_Ms that heavily depend on IL-7 and IL-15 for maintenance. It is possible that T_Ms that are sustained through other forms of regulation may exhibit other homing patterns. For instance, it has been reported that T_Ms generated from a localized infection in a peripheral tissue, such as skin, gut and lung, tend to be "imprinted" with the capacity to home back to that particular tissue.[31,32,46] It will be interesting for future study to characterize the homeostatic regulation of these T_Ms and their whole-body reservoir distribution.

Acknowledgments

The authors thank Sarkis Mazmanian and June L. Round for technical advice, and Pin Wang, Dan Kahn, Xin Luo and Shengli Hao for critical reading of this manuscript and insightful discussions.

This work was supported by the Skirball Foundation and National Institutes of Health P01 CA132681A.

Authorship

Contribution: L.Y. designed, performed and analyzed experiments, and wrote the paper; Y.Y., M.K., and T.-W.J.T. performed and analyzed experiments; and D.B. analyzed experiments and wrote the paper.

Conflict-of-interest disclosure: The authors declare no competing financial interests.

The current affiliation for T.-W.J.T. is Boehringer Ingelheim Pharmaceuticals Inc.

Correspondence: Lili Yang, Division of Biology, M/C 147-75, California Institute of Technology, 1200 E California Blvd, Pasadena, CA, 91125; e-mail: liyang@caltech.edu; or David Baltimore, Division of Biology, M/C 147-75, California Institute of Technology, 1200 E California Blvd, Pasadena, CA 91125; e-mail: baltimo@caltech.edu.

References

1. Dutton RW, Bradley LM, Swain SL. T cell memory. *Annu Rev Immunol.* 1998;16:201-223.
2. Bevan MJ. Immunology. Stimulating killer cells. *Nature.* 1989;342(6249):478-479.
3. Bishop GA, Hostager BS. B lymphocyte activation by contact-mediated interactions with T lymphocytes. *Curr Opin Immunol.* 2001;13(3):278-285.
4. Castellino F, Germain RN. Cooperation between CD4+ and CD8+ T cells: when, where, and how. *Annu Rev Immunol.* 2006;24:519-540.
5. Littman DR, Rudensky AY. Th17 and regulatory T cells in mediating and restraining inflammation. *Cell.* 2010;140(6):845-858.
6. Sakaguchi S. Naturally arising CD4+ regulatory T cells for immunologic self-tolerance and negative control of immune responses. *Annu Rev Immunol.* 2004;22:531-562.
7. Lefrancois L. Development, trafficking, and function of memory T-cell subsets. *Immunol Rev.* 2006;211:93-103.
8. Seder RA, Ahmed R. Similarities and differences in CD4+ and CD8+ effector and memory T cell generation. *Nat Immunol.* 2003;4(9):835-842.
9. Stockinger B, Bourgeois C, Kassiotis G. CD4+ memory T cells: functional differentiation and homeostasis. *Immunol Rev.* 2006;211:39-48.
10. Surh CD, Sprent J. Homeostasis of naive and memory T cells. *Immunity.* 2008;29(6):848-862.
11. Klonowski KD, Lefrancois L. The CD8 memory T cell subsystem: integration of homeostatic signaling during migration. *Semin Immunol.* 2005; 17(3):219-229.
12. Ma AR, Koka R, Burkett P. Diverse functions of IL-2, IL-15, and IL-7 in lymphoid homeostasis. *Annu Rev Immunol.* 2006;24:657-679.
13. Hataye J, Moon JJ, Khoruts A, Reilly C, Jenkins MK. Naive and memory CD4+ T cell survival controlled by clonal abundance. *Science.* 2006; 312(5770):114-116.
14. Tanchot C, Rocha B. The organization of mature T-cell pools. *Immunol Today.* 1998;19(12):575-579.
15. Becker TC, Coley SM, Wherry EJ, Ahmed R. Bone marrow is a preferred site for homeostatic proliferation of memory CD8 T cells. *J Immunol.* 2005;174(3):1269-1273.
16. Mazo IB, Honczarenko M, Leung H, et al. Bone marrow is a major reservoir and site of recruitment for central memory CD8+ T cells. *Immunity.* 2005;22(2):259-270.
17. Tokoyoda K, Zehentmeier S, Hegazy AN, et al. Professional memory CD4+ T lymphocytes preferentially reside and rest in the bone marrow. *Immunity.* 2009;30(5):721-730.
18. Cahalan MD, Parker I. Choreography of cell motility and interaction dynamics imaged by two-photon microscopy in lymphoid organs. *Annu Rev Immunol.* 2008;26:585-626.
19. Nair-Gill ED, Shu CJ, Radu CG, Witte ON. Non-invasive imaging of adaptive immunity using positron emission tomography. *Immunol Rev.* 2008; 221:214-228.
20. Negrin RS, Contag CH. In vivo imaging using bioluminescence: a tool for probing graft-versus-host disease. *Nat Rev Immunol.* 2006;6(6):484-490.
21. Yang L, Baltimore D. Long-term in vivo provision of antigen-specific T cell immunity by programming hematopoietic stem cells. *Proc Natl Acad Sci U S A.* 2005;102(12):4518-4523.
22. Szymczak AL, Workman CJ, Wang Y, et al. Correction of multi-gene deficiency in vivo using a single 'self-cleaving' 2A peptide-based retroviral vector. *Nat Biotechnol.* 2004;22(5):589-594.
23. Ahmadzadeh M, Farber DJ. Functional plasticity of an antigen-specific memory CD4 T cell population. *Proc Natl Acad Sci U S A.* 2002;99(18): 11802-11807.
24. Swain SL. Generation and in vivo persistence of polarized Th1 and Th2 memory cells. *Immunity.* 1994;1(7):543-552.
25. Williams MA, Bevan MJ. Effector and memory CTL differentiation. *Annu Rev Immunol.* 2007;25: 171-192.
26. Yang L, Yang H, Rideout K, et al. Engineered lentivector targeting of dendritic cells for in vivo immunization. *Nat Biotechnol.* 2008;26(3):326-334.
27. Kaech SM, Wherry EJ. Heterogeneity and cell-fate decisions in effector and memory CD8+ T cell differentiation during viral infection. *Immunity.* 2007;27(3):393-405.
28. Sallusto F, Geginat J, Lanzavecchia A. Central memory and effector memory T cell subsets: function, generation, and maintenance. *Annu Rev Immunol.* 2004;22:745-763.
29. Masopust D, Vezys V, Marzo AL, lefrancois L. Preferential localization of effector memory cells in nonlymphoid tissue. *Science.* 2001;291(5512): 2413-2417.
30. Bromley SK, Mempel TR, Luster AD. Orchestrating the orchestrators: chemokines in control of T cell traffic. *Nat Immunol.* 2008;9(9):970-980.
31. Mora JR, von Andrian UH. Specificity and Plasticity of Memory Lymphocyte Migration. *CTMI.* 2006;208:83-116.
32. Woodland DL, Kohlmeier JE. Migration, maintenance and recall of memory T cells in peripheral tissues. *Nat Rev Immunol.* 2009;9(3):153-161.
33. Forster R, Schubel A, Breitfeld D, et al. CCR7 coordinates the primary immune response by establishing functional microenvironments in secondary lymphoid organs. *Cell.* 1999;99(1):23-33.
34. Gallatin WM, Weissman IL, Butcher EC. A cell-surface molecule involved in organ-specific homing of lymphocytes. *Nature.* 1983;304(5921):30-34.
35. Zabel BA, Agace WW, Campbell JJ, et al. Human G protein-coupled receptor GPR-9-6/CC chemokine receptor 9 is selectively expressed on intestinal homing T lymphocytes, mucosal lymphocytes, and thymocytes and is required for thymus-expressed chemokine-mediated chemotaxis. *J Exp Med.* 1999;190(9):1241-1256.
36. Berlin C, Berg EL, Briskin MJ, et al. Alpha 4 beta 7 integrin mediates lymphocyte binding to the mucosal vascular addressin MAdCAM-1. *Cell.* 1993;74(1):185-195.
37. Wagner N, Lohler J, Kunkel EJ, et al. Critical role for beta7 integrins in formation of the gut-associated lymphoid tissue. *Nature.* 1996; 382(6589):366-370.
38. Kennedy MK, Glaccum M, Brown SN, et al. Reversible defects in natural killer and memory CD8 T cell lineages in interleukin 15-deficient mice. *J Exp Med.* 2000;191(5):771-780.
39. Reinhardt RL, Khoruts A, Merica R, Zell T, Jenkins MK. Visualizing the generation of memory CD4 T cells in the whole body. *Nature.* 2001;410(6824):101-105.
40. Hladik F, McElrath MJ. Setting the stage: host invasion by HIV. *Nat Rev Immunol.* 2008;8(6): 447-457.
41. Veazey RS, DeMaria M, Chalifoux LV, et al. Gastrointestinal tract as a major site of CD4+ T cell depletion and viral replication in SIV infection. *Science.* 1998;280(5362):427-431.
42. Li Q, Duan L, Estes JD, et al. Peak SIV replication in resting memory CD4+ T cells depletes gut lamina propria CD4+ T cells. *Nature.* 2005; 434(7037):1148-1152.
43. Mattapallil JJ, Douek DC, Hill B, Nishimura Y, Martin M, Roederer M. Massive infection and loss of memory CD4+ T cells in multiple tissues during acute SIV infection. *Nature.* 2005;434(7037): 1093-1097.
44. Shalapour S, Deiser K, Sercan O, et al. Commensal microflora and interferon-r promote steady-state interleukine-7 production in vivo. *Eur J Immunol.* 2010;40:2391-2400.
45. Masopust D, Vezys V, Marzo AL, Lefrancois L. Dynamic T cell migration program provides resident memory within intestinal epithelium. *J Exp Med.* 2010;207(3):553-564.
46. Sigmundsdottir H, Butcher EC. Environmental cues, dendritic cells and the programming of tissue-selective lymphocyte trafficking. *Nat Immunol.* 2008;9(9):981-987.

Mice and materials

C57BL/6J (B6), C57BL/6J-Tyr(c-2J)/J (Albino B6), B6.PL-Thy1a/CyJ (Thy1.1), B6.129P2-Ccr7(tm1Dgen)/J (CCR7KO), C57BL/6-Itgb7(tm1Cgn)/J (β7KO) female mice were purchased from the Jackson Laboratory (Bar Harbor, ME). C57BL/6NTac-IL15(tm1Imx) (IL-15KO) female mice were purchased from Taconic (Hudson, NY). OT1 and OT2 Tg mice were bred at Caltech. Germ-free C57BL/6J female mice were kind gift from the laboratory of Sarkis Mazmanian (Caltech). All mice were housed in the California Institute of Technology animal facility in accordance with institute regulations. $OVAp_{257-269}$ and $OVAp_{323-339}$ were purchased from GenScript (Piscataway, NJ). Polybrene were purchased from Millipore (Billerica, MA). MACS® sorting reagents were purchased from Miltenyi Biotec (Bergisch Gladbach, Germany). Recombinant murine IL-7 and IL-15 were purchased from PeproTech (Rocky Hills, NJ).

Antibodies and flow cytometry

Fluorochrome-conjugated antibodies specific for mouse CD4, CD8, TCRβ, CD25 (IL-2Rα), CD44, CD62L, CD69, CD122 (IL-2/15Rβ), CD127 (IL-7Rα), CD132 (γc), CCR4, CCR5, CCR6, CCR7, CXCR3, CXCR4, α4β7, α4 and β7 were purchased from Biolegend (San Diego, CA); for mouse TCR Vβ5, IFN-γ, IL-4 and IL-17A, from BD Biosciences (San Jose, CA); for mouse CCR9 and CCR10, from R&D Systems (Minneapolis, MN). Biotin-conjugated anti-mouse IL-15Rα was purchased from R&D Systems (Minneaplis, MN). Fc Block (anti-mouse CD16/32) and fluorochrome-conjugated Streptavidin were purchased from Biolegend (San Jose, CA). Cells were stained and analyzed using a FACSCalibur flow cytometer (BD Biosciences, San Jose,

CA) as previously described[21]. A FlowJo software (FlowJo, Ashland, OR) was used to analyze the data.

Tissue lymphocytes isolation

Lymphocytes were isolated from spleen, LNs and lung using mechanical disruption. To isolate lymphocytes from gut, at first PPs were dissected out, and were mechanically disrupted to release lymphocytes (PP lymphocytes); then the entire gut tract, from stomach to colon, was cut into small pieces, and was treated with Cell Dissociation Solution (Ca^{++} and Mg^{++} free 1xHBSS + 5mM EDTA + 10mM HEPES) (HBSS and HEPES were purchased from Invitrogen/Gibco, Carlbad, CA; EDTA was purchased from Applied Biosystems/Ambion, Austin, TX) twice for 20mins at 37°C with slow rotation at 100rpm, to isolate IELs (intra-epithelia lymphocytes); the remaining gut tissue was then treated with RPMI (Fisher Scientific, Pittsburgh, PA) containing 10% FBS (Omega Scientific, Tarzana, CA) and 0.5mg/ml Collagenase Type II (SIGMA-ALDRICH®, St. Louis, MO) twice for 30min at 37°C with slow rotation at 100rpm, to isolate LPLs (lamina propria lymphocytes). BM cells were flushed out from bones that had both ends cut open.

DC-directed lentivirus infection

DC-directed lentivirus expressing OVA antigen (FOVA/SVGm), or an engineered OVA that favors the MHC class II presentation (FMOVA/SVGm) were generated as previously described[26]. OT1 or OT2 Tg mice were infected with $1x10^8$ TU either FKOVA/SVGm or FMOVA/SVGm lentivirus through footpad injection, respectively. The mice were analyzed for the presence of T_Ms 2 months post the infection.

CD4 T_Es differentiation *in vitro*

SP and LN cells harvested from B6 female mice were cultured in T cell culture media containing 0.5μg/ml anti-mouse CD3 and 0.5μg/ml anti-mouse CD28 for 3 days, in the absence (for T_H0 culture) or presence of the following supplements: 10ng/ml recombinant murine IL-12 and 10μg/ml anti-mouse IL-4 (for T_H1 differentiation);

400ng/ml recombinant murine IL-4, 10μg/ml anti-mouse IFN-γ and 10μg/ml anti-mouse IL-12/IL-23 P40 (for T_H2 differentiation); 20ng/ml recombinant murine IL-6, 5ng/ml recombinant human TGF-β1, 10μg/ml anti-mouse IL-4 and 10μg/ml anti-mouse IFN-γ (for T_H17 differentiation). All the recombinant proteins were purchased from PeproTech (Rocky Hill, NJ). All the antibodies were purchased from Biolegend (San Diego, CA).

CD4 T_Ms functional analysis

Cells were stimulated with 50ng/ml PMA and 500ng/ml Ionomycin (EMD Biosciences, San Diego, CA) for 6 hours in the presence of 1μl/ml BD GolgiPlug™ (BD Biosciences, San Diego, CA). Cytokine production was then analyzed *via* intracellular staining using BD Cytofix/Cytoperm™ Fixation/Permeabilization Kit (BD Biosciences, San Diego, CA) according to manufacturer's protocol.

IL-7 and IL-15 mRNA tissue expression

Mouse tissues were homogenized using a PowerGen 500 homogenizer (Fisher Scientific, Pittsburgh, PA). Tissue RNA was then extracted using TRIzol® Reagent and cDNA was synthesized using SuperscriptII Reverse Transcriptase according to manufacturer's protocols (Invitrogen, Carlsbad, CA). Q-PCR was performed on a 7300 Real-Time PCR system using TaqMan® Gene Expression Assays kits designed for murine IL-7 and IL-15, according to manufacturer's instructions (Applied Biosystems, Foster City, CA). The IL-7 and IL-15 mRNA levels in various tissues were normalized to the β-actin levels.

Figure S1. Phenotype of antigen-specific and polyclonal T cells prior to and post-adoptive transfer of *in vitro* differentiated effector T cells (T_Es) labeled with MFG, related to Fig. 1

(A) Purity and MFG labeling efficiency of *in vitro* differentiated OVA-specific OT1 and OT2 T_Es sorted using MACS. Spleen and LN cells harvested from 8-week old OT1 or OT2 transgenic mice were stimulated with their cognate OVA peptides *in vitro* for 3 days and transduced with MFG. OT1 and OT2 T_Es were then purified using MACS, and analyzed using flow cytometry for their purity (gated as $CD8^+V\beta5^+$ and $CD4^+V\beta5^+$, respectively) and MFG labeling efficiency (gated as $CD8^+GFP^+$ and $CD4^+GFP^+$, respectively).

(B) Surface activation marker expression on OVA-specific OT1 and OT2 T cells at various stages analyzed by flow cytometry. Representative histogram plots of resting OT1 and OT2 T cells (gated as $CD8^+V\beta5^+$ and $CD4^+V\beta5^+$, respectively) freshly isolated from the spleen of 8-week old OT1 or OT2 transgenic mice, the *in vitro* differentiated OT1 and OT2 T_Es transduced with MFG (gated as $CD8^+V\beta5^+GFP^+$ and $CD4^+V\beta5^+GFP^+$, respectively) prior to adoptive transfer, and the MFG-labeled OT1 and OT2 T_Ms (gated as $CD8^+V\beta5^+GFP^+$ and $CD4^+V\beta5^+GFP^+$, respectively) isolated from the spleen of recipient mice two months post adoptive transfer of T_Es are shown (n>4).

(C) Purity and MFG labeling efficiency of *in vitro* differentiated polyclonal CD4 and CD8 T_Es sorted using MACS. Spleen and LN cells harvested from 8-week old B6 mice were stimulated with 1μg/ml anti-CD3 and 1μg/ml anti-CD28 *in vitro* for 3 days and transduced with MFG. CD4 and CD8 T_Es were then purified using MACS, and analyzed using flow cytometry for their purity (gated as $CD4^+$ and $CD8^+$, respectively) and MFG labeling efficiency (gated as $CD4^+GFP^+$ and $CD8^+GFP^+$, respectively).

(B) Surface activation marker expression on polyclonal CD4 and CD8 T cells at various stages analyzed by flow cytometry. Representative histogram plots of resting CD4 and CD8 T cells (gated as $CD4^+$ and $CD8^+$, respectively) freshly isolated from the spleen of 8-week old B6 mice, the *in vitro* differentiated polyclonal CD4 and CD8 T_Es transduced

with MFG (gated as $CD4^+GFP^+$ and $CD8^+GFP^+$, respectively) prior to adoptive transfer, and the MFG-labeled polyclonal CD4 and CD8 T_Ms (gated as $CD4^+GFP^+$ and $CD8^+GFP^+$, respectively) isolated from the spleen of recipient mice two months post adoptive transfer of T_Es are shown (n>4).

Figure S2. Tracking the tissue homing of OT2 and OT1 T cells during their transition from T_Es to T_Ms using dissected tissue BLI, related to Fig. 1

$3x10^6$ MFG-labeled OT2 or OT1 T_Es were adoptively transferred into each albino B6 recipient mouse. BLI images collected 1 day (A) and 1 week (B) post the adoptive transfer are shown. Data are representative of 3 independent experiments. PLN: peripheral lymph node; MLN: mesenteric lymph node; SP: spleen; BM: bone marrow; Pan: pancreas; Savi: salivary gland; Ty: thymus.

Figure S3.Tissue distribution of various CD4 and CD8 T_Ms, related to Fig. 2

(A) Representative flow cytometry data for the quantification of CD4 and CD8 T_Ms (gated as $Thy1.2^+CD4^+$ and $Thy1.2^+CD8^+$, respectively) generated in Thy1.1 congenic mice 2 months post-transfer of a mix of equal number ($10x10^6$) of B6 CD4 and CD8 T_Es. N=4. Related to Figure 2A upper.

(B) Representative flow cytometry data and cell number counts (mean ± SEM) for the quantification of memory-phenotype (MP) CD4 T_Ms (gated as $CD4^+CD25^-CD44^{hi}$, CD25 staining was included to gate off Tregs) and CD8 T_Ms (gated as $CD8^+TCR\beta^+CD44^{hi}$, TCRβ staining was included to gate off the $CD8^+$ non-αβ T cells in some tissues) spontaneously generated in 1-year old B6 mice. CD62L staining was used to distinguish between T_{CM} ($CD62L^+$) and T_{EM} ($CD62L^-$). N=4. Related to Figures 2A middle and 2B.

(C) Representative flow cytometry data for the quantification of OVA-specific OT2 and OT1 T_Ms (gated as $CD4^+CD25^-TCRV\beta5^+CD44^{hi}$ and $CD8^+TCRV\beta5^+CD44^{hi}$, respectively) generated in OT2 or OT1 transgenic mice 2 months post infection with $1x10^8$ TU DC-directed lentivirus expressing OVA antigen. N=4. Related to Figure 2A lower.

(D) Distribution of MP CD4 and CD8 T_M in various gut compartments. Cells were harvested from the intra-epithelial (IE), lamina propria (LP) and Peyer's Patches (PPs) compartments of the gut of 1-year old B6 mice, and were analyzed for the presence of MP CD4 and CD8 T_Ms (gated as $CD4^+CD25^-CD44^{hi}$ and $CD8^+TCR\beta^+CD44^{hi}$, respectively) using flow cytometry. Data are presented as mean ± SEM (n=4). Similar results were observed for B6 mice aged from 3 months to 1 year. Note that IE is slightly biased for CD8 T_M accumulation. However, since IE only comprises a small portion of gut, the overall gut is still strongly biased for CD8 T_M accumulation.

(E) Tissue distribution of CD4 and CD8 naïve T cells (T_Ns). Cells were harvested from the various tissues of 9-month old B6 mice, and were analyzed for the presence of CD4 and CD8 T_Ns (gated as $CD4^+CD25^-CD44^{lo}$ or $CD8^+TCR\beta^+CD44^{lo}$, respectively) using flow cytometry. Data are shown as mean ± SEM (n=4). Similar results were observed for B6 mice aged from 3 months to 1 year. PLN: peripheral LN; PanLN: pancreatic LN; CLN: cervical LN; LumLN: lumbar LN; MLN: mesenteric LN; RenLN: renal LN; TyLN: thymic LN; BM: bone marrow; SP: spleen; PB: peripheral blood; Ty: thymus.

(F) Tissue distribution of CD4 and CD8 T_{CM}s and T_{EM}s. Various tissues were harvested from 1-year old B6 mice and analyzed for the presence of MP CD4 and CD8 T_{CM}s and T_{EM}s (gated as $CD4^+CD25^-CD44^{hi}CD62L^+$, $CD4^+CD25^-CD44^{hi}CD62L^-$, $CD8^+TCR\beta^+CD44^{hi}CD62L^+$ or $CD8^+TCR\beta^+CD44^{hi}CD62L^-$, respectively) using flow cytometry. Representative histogram plots of T_Ms harvested from the indicated tissues

are shown (n=4). T_{CM}s: central memory T cells; T_{EM}s: effector memory T cells. Note that selective histogram plots are also shown in Figure 2B.

Figure S4. Homing marker expression on various T_Ms, related to Fig. 3

(A) Homing marker expression on CD4 and CD8 T_Ms analyzed by flow cytometry.

(Upper) OVA antigen-specific OT2 and OT1 T_Ms (gated as Thy1.2$^+$CD4$^+$Vβ5$^+$ and Thy1.2$^+$CD8$^+$Vβ5$^+$, respectively) detected in the spleen of Thy1.1 congenic mice 2 months post adoptive transfer of 10x10^6 *in vitro* differentiated OT2 or OT1 T_Es.

(Middle) Polyclonal CD4 and CD8 T_Ms (gated as Thy1.2$^+$CD4$^+$ and Thy1.2$^+$CD8$^+$, respectively) detected in the spleen of Thy1.1 congenic mice 2 months post adoptive transfer of a mix of equal number (10x10^6) of B6 CD4 and CD8 T_Es.

(Lower) OVA antigen-specific OT2 and OT1 T_Ms (gated as CD4$^+$CD25$^-$TCRVβ5$^+$CD44^{hi} and CD8$^+$TCRVβ5$^+$CD44^{hi}, respectively) detected in the spleen of OT2 or OT1 transgenic mice 2 months post infection with 1x10^8 TU DC-directed lentivirus expressing OVA antigen.

Representative histogram plots are shown (n=4).

(B) Flow cytometry analysis of other homing marker expression on MP CD4 and CD8 T_Ms harvested from the spleen of 1-year old B6 mice (gated as CD4$^+$CD25$^-$CD44^{hi} and CD8$^+$CD44^{hi}, respectively). Representative histogram plots and measurements of mean fluorescence intensity (MFI) are shown (n=4).

(C) Representative flow cytometry data showing the time-course tracking of CD4 and CD8 T cells (gated as Thy1.2$^+$CD4$^+$ and Thy1.2$^+$CD8$^+$, respectively) in the indicated tissues of Thy1.1 congenic mice post-transfer of a mix of equal number (10x10^6) of B6 CD4 and CD8 T_Es (n=4).

Figure S5. Cytokine receptor expression on antigen-specific T_Ms and on T cells at various activation stages, related to Fig. 5

(A) Cytokine receptor expression on CD4 and CD8 T cells at naïve (T_N), effector (T_E) and memory (T_M) stages measured by flow cytometry. CD4 and CD8 T_Ns (gated as $CD4^+CD25^-CD44^{lo}$ or $CD8^+CD44^{lo}$, respectively) and MP T_Ms (gated as $CD4^+CD25^-CD44^{hi}$ or $CD8^+CD44^{hi}$, respectively) were identified from the spleen of 1-year old B6 mice. T_Es were generated by stimulating the B6 spleen cells with anti-CD3 and anti-CD28 for 3 days *in vitro*. Representative histogram plots and measurements of mean fluorescence intensity (MFI) are shown (n>4).

(B) Time-course tracking of IL-2/15Rβ expression on CD4 and CD8 T cells during their transition from T_Es to T_Ms. A mix of equal number ($10x10^6$) of B6 CD4 and CD8 T_Es were transferred into each Thy1.1 congenic recipient mouse. At the indicated time points post adoptive transfer, B6 CD4 and CD8 T cells (gated as $Thy1.2^+CD4^+$ or $Thy1.2^+CD8^+$, respectively) in the spleen of recipients were analyzed for their expression of IL-2/15Rβ using flow cytometry. Representative histogram plots (upper) and measurements of the mean fluorescence intensity (MFI) (lower) are shown (n=3). Shaded area marks contraction phase.

Figure S6. Homeostatic cytokines regulate the differentiated expression of gut-homing markers on CD4 and CD8 T_Ms *in vitro* and *in vivo*, related to Fig. 6

(A) MP CD4 and CD8 T_Ms (gated as $CD4^+CD25^-CD44^{hi}$ and $CD8^+CD44^{hi}$, respectively) harvested from the spleen of 9-month old IL-15KO mice with or without IL-15 administration (i.p. 10μg daily for 5 sequential days) were analyzed for their expression of IL-2/15Rβ, and PLN- and gut-homing markers using flow cytometry. Representative data are shown as histogram plots and measurements of mean fluorescence intensity (n=3).

(B) Representative flow cytometry data for the quantification of MP CD4 and CD8 T_Ms (gated as $CD4^+CD25^-CD44^{hi}$ and $CD8^+TCR\beta^+CD44^{hi}$, respectively) in the PLNs and PPs of 9-month old IL-15KO mice with or without supplementation of IL-15 (i.p.10μg daily for 5 sequential days) (n=3). Related to Figures 6B-6C.

(C) Comparison of gut-homing marker expression on MP CD4 and CD8 T_Ms (gated as $CD4^+CD25^-CD44^{hi}$ and $CD8^+CD44^{hi}$, respectively) harvested from the SP and PLNs of 1-year old B6 mice using flow cytometry. Histogram plots and measurements of mean fluorescence intensity are shown. Data are representative of at least 3 independent experiments.

Figure S7. Tissue distribution of CD4 and CD8 T_Ms in germ-free (GF) mice, related to Fig. 7

Various tissues were harvested from 6-month old germ-free (GF) B6 mice or regular wild-type (WT) B6 mice and analyzed for the presence of MP CD4 and CD8 T_Ms (gated as $CD4^+CD25^-CD44^{hi}$ and $CD8^+CD44^{hi}$, respectively) using flow cytometry.

(A) Representative flow cytometry data for the quantification of MP CD4 and CD8 T_Ms in the PP of WT and GF B6 mice (n=4).

(B) Tissue accumulation of MP CD4 and CD8 T_Ms in WT and GF B6 mice. Data are presented as mean ± SEM (n=4).

(C) Comparison of MP CD4 and CD8 T_M cell number in PLN and PP of WT and GF B6 mice. Data are presented as mean ± SEM (n=4).

Figure S1 (related to Fig. 1)

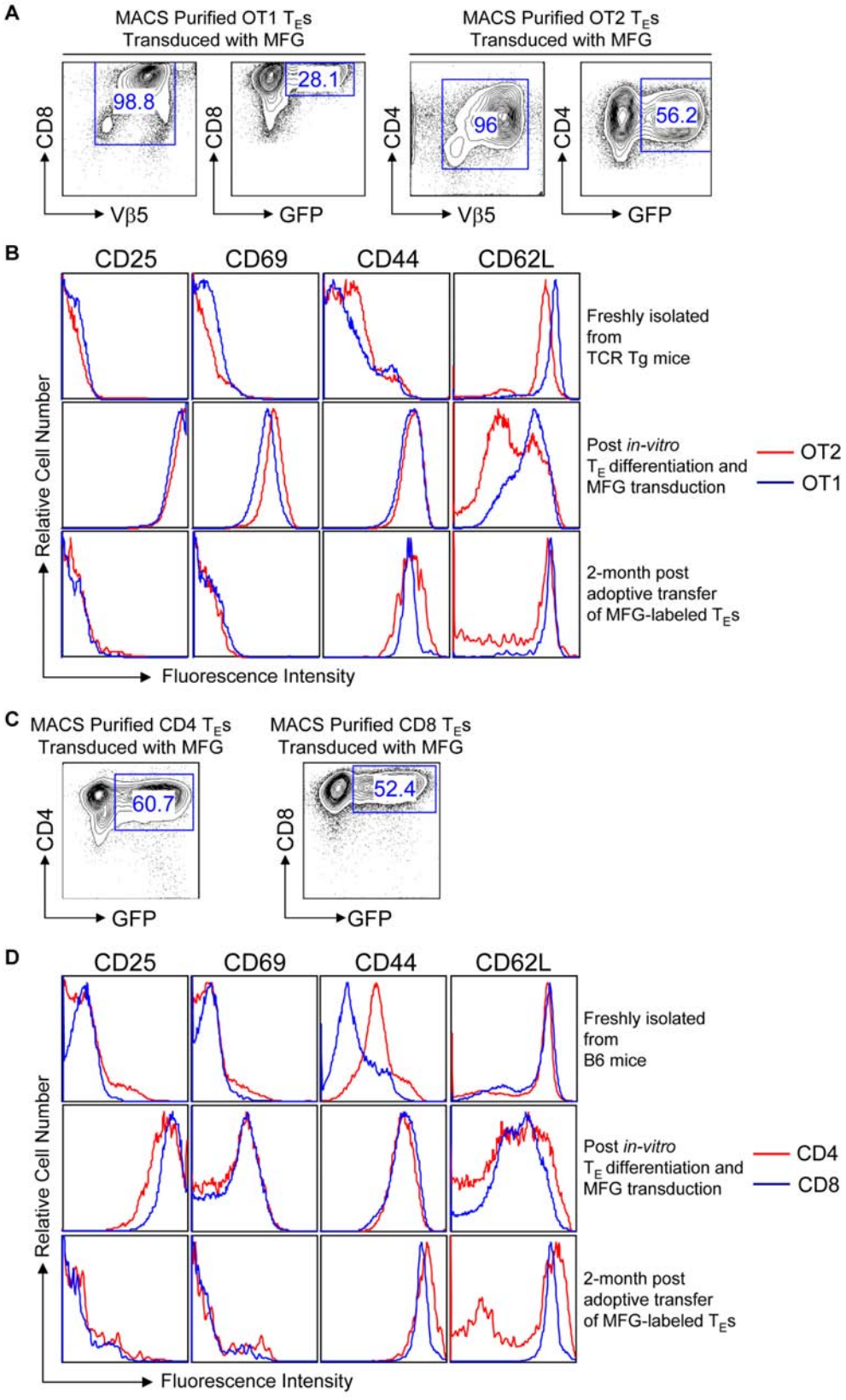

Figure S2 (related to Fig. 1)

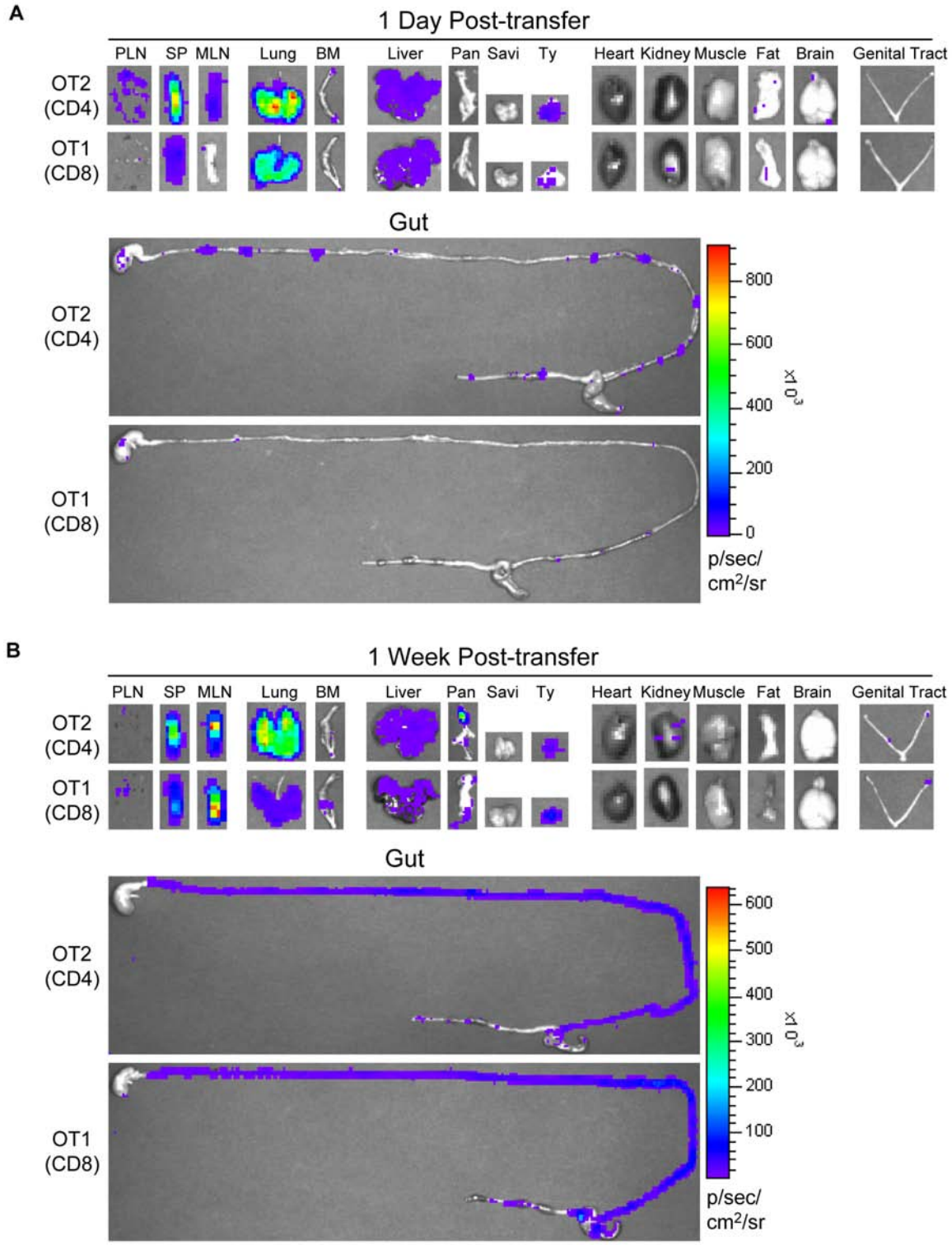

Figure S3 (related to Fig. 2)

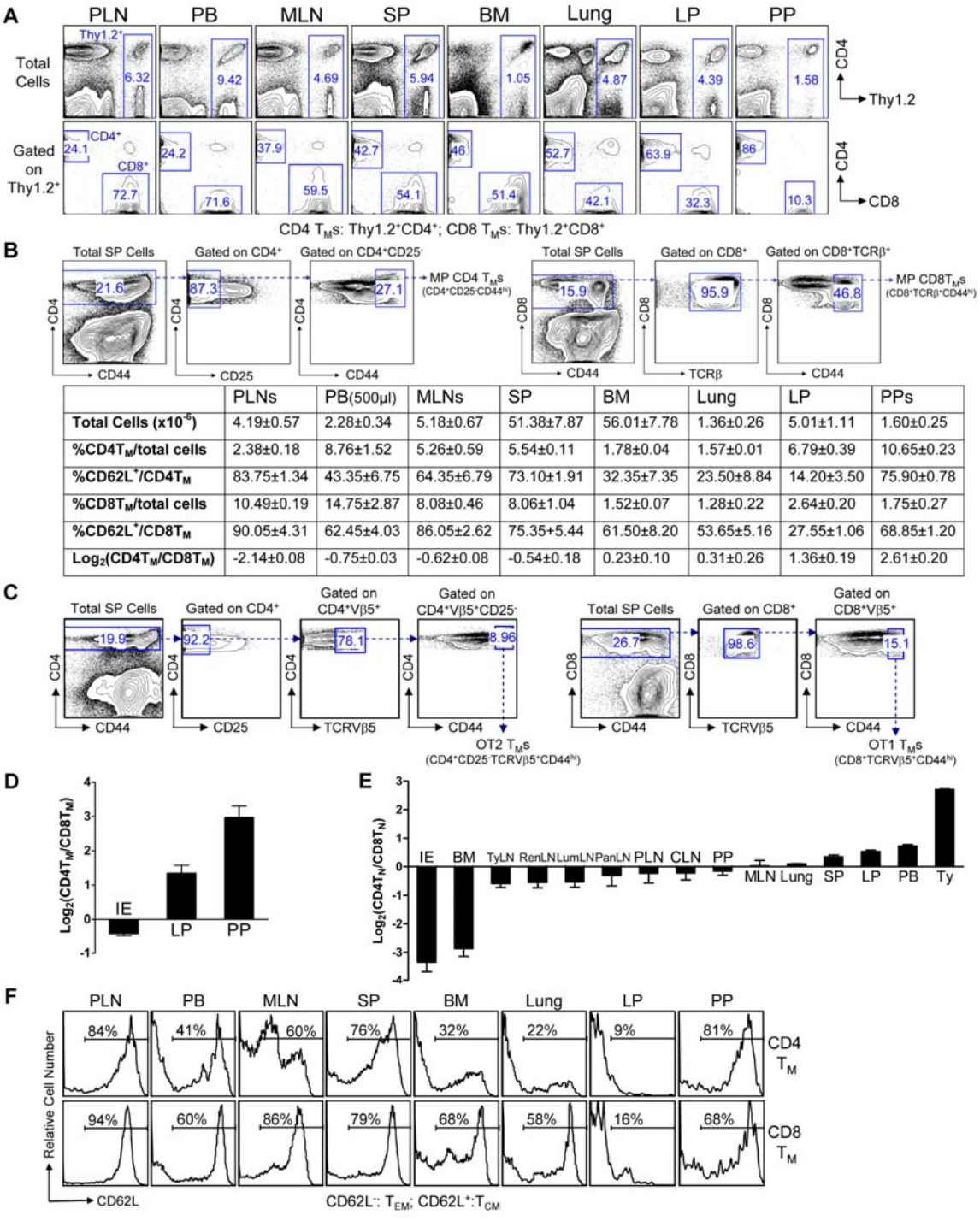

	PLNs	PB(500μl)	MLNs	SP	BM	Lung	LP	PPs
Total Cells (x10^{-5})	4.19±0.57	2.28±0.34	5.18±0.67	51.38±7.87	56.01±7.78	1.36±0.26	5.01±1.11	1.60±0.25
%CD4T$_M$/total cells	2.38±0.18	8.76±1.52	5.26±0.59	5.54±0.11	1.78±0.04	1.57±0.01	6.79±0.39	10.65±0.23
%CD62L$^+$/CD4T$_M$	83.75±1.34	43.35±6.75	64.35±6.79	73.10±1.91	32.35±7.35	23.50±8.84	14.20±3.50	75.90±0.78
%CD8T$_M$/total cells	10.49±0.19	14.75±2.87	8.08±0.46	8.06±1.04	1.52±0.07	1.28±0.22	2.64±0.20	1.75±0.27
%CD62L$^+$/CD8T$_M$	90.05±4.31	62.45±4.03	86.05±2.62	75.35+5.44	61.50±8.20	53.65±5.16	27.55±1.06	68.85±1.20
Log$_2$(CD4T$_M$/CD8T$_M$)	-2.14±0.08	-0.75±0.03	-0.62±0.08	-0.54±0.18	0.23±0.10	0.31±0.26	1.36±0.19	2.61±0.20

Figure S4 (related to Fig. 3)

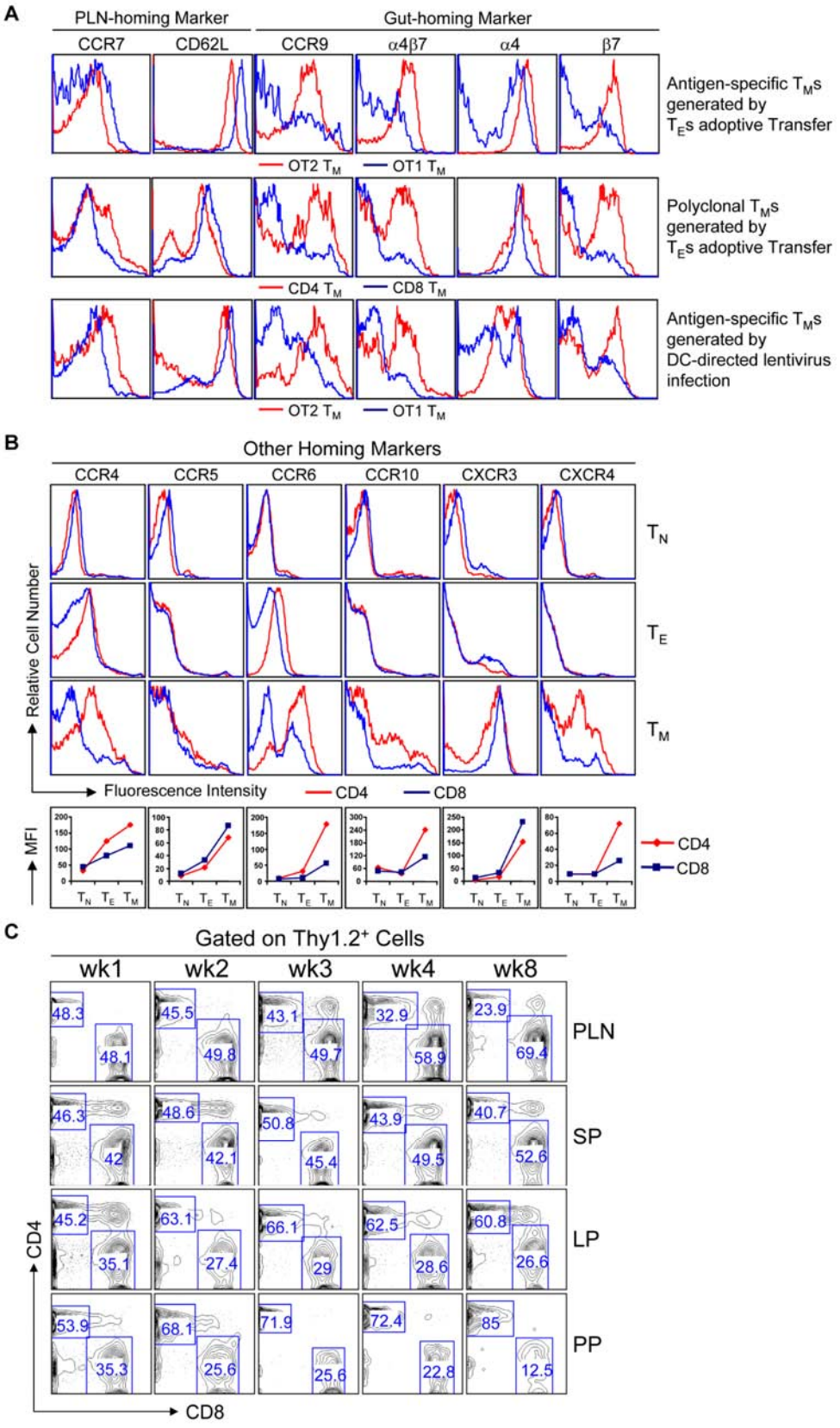

Figure S5 (related to Fig. 5)

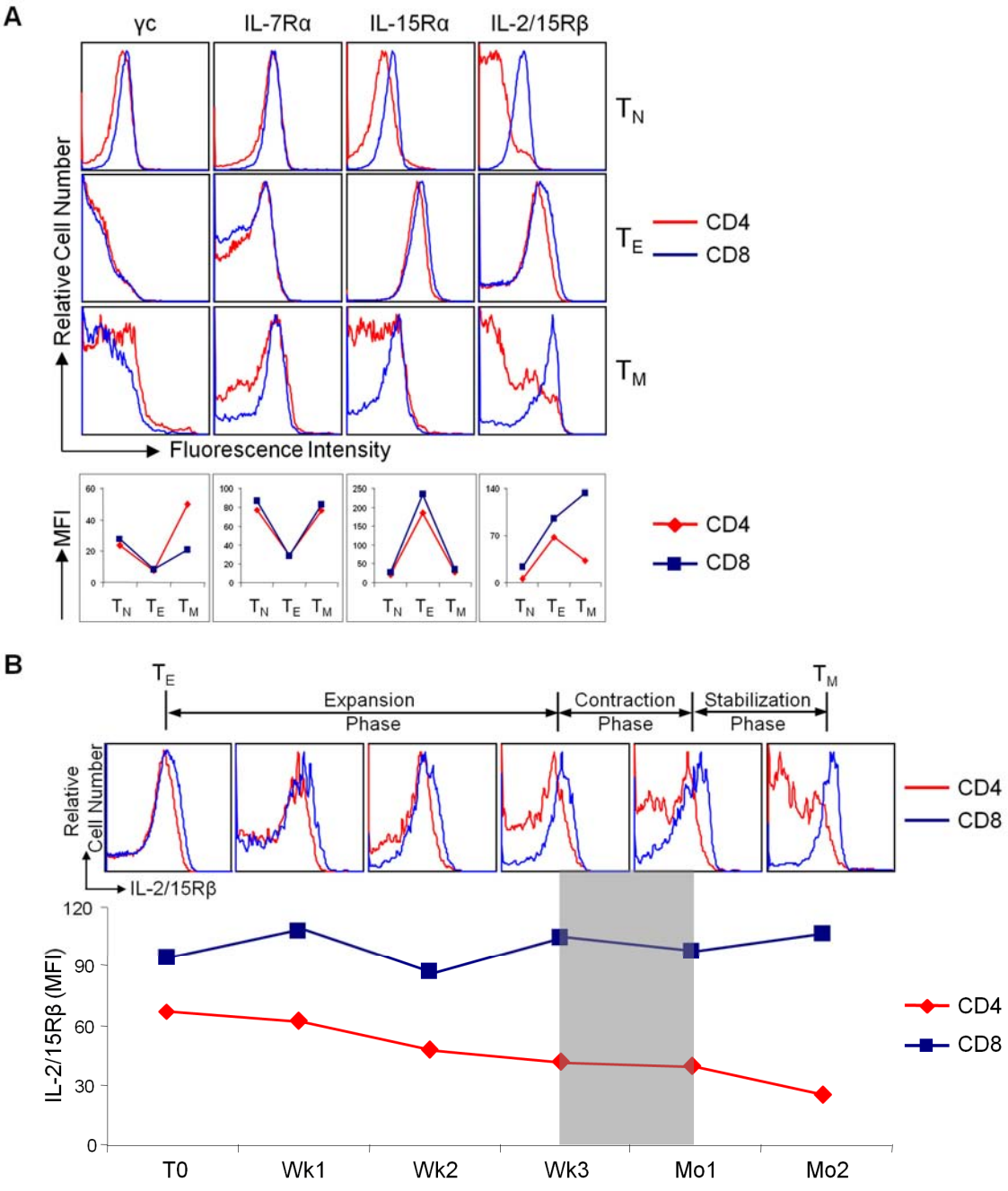

Figure S6 (related to Fig. 6)

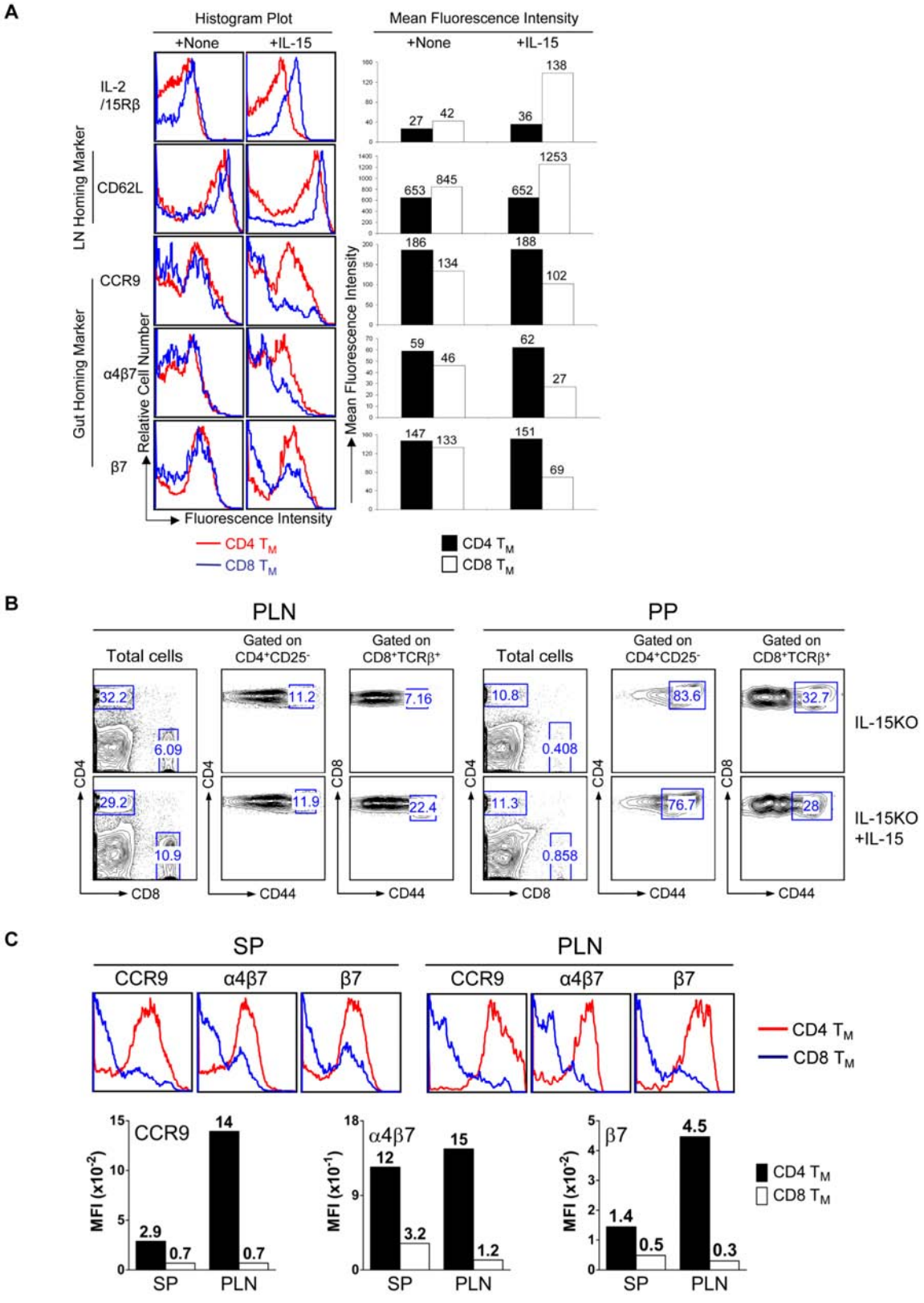

Figure S7 (related to Fig. 7)